



HAL
open science

Copolymerization of ethylene with propylene and higher α -olefins catalyzed by (imido)vanadium(iv) dichloride complexes

Giorgia Zanchin, Fabio Bertini, Laure Vendier, Giovanni Ricci, Christian Lorber, Giuseppe Leone

► To cite this version:

Giorgia Zanchin, Fabio Bertini, Laure Vendier, Giovanni Ricci, Christian Lorber, et al.. Copolymerization of ethylene with propylene and higher α -olefins catalyzed by (imido)vanadium(iv) dichloride complexes. *Polymer Chemistry*, 2019, 10 (45), pp.6200-6216. 10.1039/C9PY01415B . hal-02376265

HAL Id: hal-02376265

<https://hal.science/hal-02376265v1>

Submitted on 27 Oct 2020

HAL is a multi-disciplinary open access archive for the deposit and dissemination of scientific research documents, whether they are published or not. The documents may come from teaching and research institutions in France or abroad, or from public or private research centers.

L'archive ouverte pluridisciplinaire **HAL**, est destinée au dépôt et à la diffusion de documents scientifiques de niveau recherche, publiés ou non, émanant des établissements d'enseignement et de recherche français ou étrangers, des laboratoires publics ou privés.

Polymer Chemistry

Accepted Manuscript

This article can be cited before page numbers have been issued, to do this please use: G. Zanchin, F. Bertini, L. Vendier, G. Ricci, C. Lorber and G. Leone, *Polym. Chem.*, 2019, DOI: 10.1039/C9PY01415B.



This is an Accepted Manuscript, which has been through the Royal Society of Chemistry peer review process and has been accepted for publication.

Accepted Manuscripts are published online shortly after acceptance, before technical editing, formatting and proof reading. Using this free service, authors can make their results available to the community, in citable form, before we publish the edited article. We will replace this Accepted Manuscript with the edited and formatted Advance Article as soon as it is available.

You can find more information about Accepted Manuscripts in the [Information for Authors](#).

Please note that technical editing may introduce minor changes to the text and/or graphics, which may alter content. The journal's standard [Terms & Conditions](#) and the [Ethical guidelines](#) still apply. In no event shall the Royal Society of Chemistry be held responsible for any errors or omissions in this Accepted Manuscript or any consequences arising from the use of any information it contains.

Copolymerization of Ethylene with Propylene and Higher α -Olefins Catalyzed by (Imido)vanadium(IV) Dichloride Complexes

Giorgia Zanchin,[†] Fabio Bertini,[†] Laure Vendier,^{1,#}
Giovanni Ricci,[†] Christian Lorber,^{1,#,*} and Giuseppe Leone^{†,*}

[†] CNR, Istituto di Scienze e Tecnologie Chimiche “Giulio Natta” (SCITEC), via A. Corti 12, I-20133 Milano, Italy.

¹ CNRS, LCC (Laboratoire de Chimie de Coordination), 205 route de Narbonne, BP44099, 31077 Toulouse, France

[#] Université de Toulouse, UPS, INPT, LCC, 31077 Toulouse, France

* Corresponding authors

E-mail address: christian.lorber@lcc-toulouse.fr (C. Lorber)

E-mail address: giuseppe.leone@ismac.cnr.it (G. Leone)

Keywords: ethylene, propylene, copolymerization, vanadium, polyolefins

ABSTRACT

View Article Online
DOI: 10.1039/C9PY01415B

We have synthesized and characterized a series of dimethylamine–imido $V(=NR)Cl_2(NHMe_2)_2$ [$R = tBu$ (**1a**), CPh_3 (**1b**), 2,6- $CHPh_2$ -4- $Cl-C_6H_2$ (**1c**)], and pyridine–imido $V(=NR)Cl_2(Py)_3$ [$R = tBu$ (**2a**), CPh_3 (**2b**), 2,6- $CHPh_2$ -4- $Cl-C_6H_2$ (**2c**)] complexes. The solid-state structure of **1a–1c**, and **2c** was determined by X-ray crystallography. Complexes **1a**, and **2a–2c**, in combination with Et_2AlCl and Cl_3CCO_2Et , have been screened as catalysts for the copolymerization of ethylene with various α -olefins (*i.e.*, propylene, 1-hexene, 1-octene, and 4-methyl-1-pentene). The results are compared with the known PMe_2Ph –imido $V(=NR)Cl_2(PMe_2Ph)_2$ [$R = tBu$ (**3a**), 2,6- $iPr_2-C_6H_3$ (**3d**)] complexes. Differences in the (co)polymerization regarding the activity and reactivity toward the target comonomers are investigated to probe the effect of imido ligand substitution, and of the coligand. With the exception of dimethylamine **1a**, **2** and **3** are instantaneously activated and exhibit good activity, affording copolymers with a moderate comonomer content ($4.2 < mol\% < 13.7$), from low to high molecular weight ($36 < M_w \times 10^3 \text{ g mol}^{-1} < 270$), and unimodal molecular weight distribution ($2.1 < M_w/M_n < 2.7$), strongly depending on the type of comonomer, copolymerization temperature, and, to a lesser extent, by the type of ligand set employed. ^{13}C NMR spectra of poly(ethylene-*co*-propylene)s have been fully interpreted as the result of uninterrupted methylene sequence distribution, ethylene–propylene sequence, and inverted propylene units. In addition, the copolymers were characterized by DSC, TGA, and successive self-nucleation and annealing (SSA). A preliminary investigation of the copolymers tensile behavior was performed by uniaxial stretching until failure.

INTRODUCTION

The worldwide production of polyolefins accounts for half of 348 million tons of the global plastics production.¹ Polyolefins continue to experience an ever-growing demand in a myriad of products that benefit our society, such as packaging, building and construction, medical applications, lightweight engineering plastics for automotive, electrical and thermal insulation. At the present time, more than 300 diverse polyolefin grades are available on the market. Among them, ethylene (co)polymers differ from each other in terms of the ratio between the (co)monomers, microstructure, stereochemistry, branching (type and amount), molecular weight, and molecular weight distribution, which in turn strongly affect physical, mechanical and rheological properties of these materials.^{2,3}

The field of olefins (co)polymerization has been the subject of intense research by numerous academic,⁴⁻⁷ and industrial laboratories,⁸⁻¹⁰ but the development of even more high-performance polyolefins will continue in the next years driven by (i) advancement in transition metal catalysts, (ii) the ever-increasing understanding of mechanistic aspects, (iii) reaction engineering, and (iv) polymer processing. Although most polyolefins are still produced using traditional Ziegler–Natta catalysts (Ti, and Cr catalysts on solid supports), billions of pounds of different poly(ethylene) (PE) grades are currently produced annually by using molecular catalysts. Molecular catalysts for (co)polymerization of ethylene typically contain electrophilic, high-valent, unsaturated metal centres, these each coordinate to the monomer, which then undergoes insertion into a metal–alkyl bond. The discovery of *ansa*–metallocenes in the 1980s marked a milestone: indeed, it allowed chemists to make significant progress in understanding the relationship between structure, activity, and stereochemistry in olefin (co)polymerization.¹⁰⁻¹² Afterwards, this interest expanded to catalysis through well-defined transition metal complexes with other ligand motifs:¹³⁻¹⁵ this has led to extraordinary advances in producing new products for advanced applications.

Amongst the transition metal series, Group IV,¹⁶ chromium,^{17,18} and late metal (particularly Ni and Pd)¹⁹ based catalysts have been highly documented. On the other hand, vanadium complexes

have been less investigated as catalyst precursors for olefin (co)polymerization, despite they have been the workhorse for the manufacture of ethylene-propylene rubber (EPR),²⁰ and ethylene-propylene-diene elastomer (EPDM).²¹

The recent resurgence of vanadium stems from the use of Schiff-base phenoxyimine-type ligands by Fujita at Mitsui.¹³ Since then, a set of vanadium complexes supported by mono- and multi-dentate ligands,²²⁻²⁴ including phenoxyimines,²⁵ aryloxides,²⁶ β -enaminoketonato,²⁷ diamine-bis(phenolate),²⁸ bis(arylimo)acenaphthene,²⁹ phosphine,³⁰⁻³² oxazoline,³³ and *N*-heterocyclic carbenes³⁴ have been successfully developed. In this framework, we recently reported the synthesis of a set of phosphine adducts of (imido)V(IV) complexes, and we demonstrated their successful application as catalyst precursors for the copolymerization of ethylene with cyclic olefins.³⁵ Herein, to expand our study on this family of complexes, we report the synthesis, and the characterization of a series of dimethylamine-imido V(=NR)Cl₂(NHMe₂)₂ [R = *t*Bu (**1a**), CPh₃ (**1b**), 2,6-CHPh₂-4-Cl-C₆H₂ (**1c**), and pyridine-imido V(=NR)Cl₂(Py)₃ [R = *t*Bu (**2a**), CPh₃ (**2b**), 2,6-CHPh₂-4-Cl-C₆H₂ (**2c**)] complexes, and their application, in combination with Et₂AlCl and Cl₃CCO₂Et (ETA), as catalysts in the (co)polymerization of ethylene with α -olefins (*i.e.*, propylene, 1-hexene, 1-octene, and 4-methyl-1-pentene). Copolymerization experiments with the known PMe₂Ph-imido complexes of the general formula V(=NR)Cl₂(PMe₂Ph)₂ [R = *t*Bu (**3a**), R = 2,6-*i*Pr₂-C₆H₃ (**3d**)],³⁵ were performed as well for comparison. The (co)polymers have been characterized by NMR, DSC, TGA, and SSA, a thermal fractionation technique based on sequential application of self-nucleation and annealing steps. A preliminary investigation of the copolymers tensile behavior was performed by uniaxial stretching until failure.

EXPERIMENTAL

General procedures and materials

Manipulations of air- and/or moisture-sensitive materials were carried out under an inert atmosphere using a dual vacuum/nitrogen line and standard Schlenk-line techniques or in a glove box filled with argon. Ethylene, propylene and nitrogen were purified by passage over columns of

CaCl₂ and molecular sieves; oxygen was removed by fluxing the gases through BTS catalysts. Before being used in polymerization, the required amount of propylene was condensed into a 25 mL Schlenk flask kept in liquid nitrogen, then toluene was added and the stabilized propylene solution was brought to room temperature. Toluene (Aldrich, ≥99.7%) was refluxed over Na for 8 hours and then distilled, and stored over molecular sieves. Dichloromethane (Aldrich, ≥99.8%) was dried by stirring over CaH₂ in inert atmosphere for 8 hours, distilled, and stored over 5 Å molecular sieves away from bright light. Ethyltrichloroacetate (ETA, Aldrich, 97%) was dried by stirring for about 4 hours and then distilled under reduced pressure. Diethylaluminium chloride (Et₂AlCl, Aldrich) was used as received. 1-Hexene (Aldrich, 97% pure), 1-octene (Aldrich, 98% pure) and 4-methyl-1-pentene (Aldrich, 98% pure) were dried by stirring over CaH₂ for about 4 hours, then distilled under reduced pressure and, finally, stored under dry nitrogen and kept at -30 °C. V(NMe₂)₄ was prepared by a modification of a literature procedure.³⁶ Pyridine and ^tBuNH₂ were dried over KOH, refluxed over CaH₂, distilled, and stored over 4 Å molecular sieves under argon before use. Trimethylchlorosilane was distilled and stored over 4 Å molecular sieves under argon before use. Compounds [V(=NR)Cl₂(PMe₂Ph)₂] [R = ^tBu (**3a**), and 2,6-ⁱPr₂-C₆H₃ (**3d**)] were prepared according to our published procedure.^{35,37} Aniline 2,6-(Ph₂CH)₂-4-Cl-C₆H₂ (**Ar**NH₂**) was prepared according to a known synthesis,³⁸ and carefully dried first in dichloromethane solution under MgSO₄, and then in the solid state in a desiccator with P₂O₅ under vacuum, and stored in the glove box before use.

Synthesis of Vanadium Complexes

*Synthesis of [V(=N^tBu)Cl₂(NHMe₂)₂] (**1a**)*

This compound was prepared by a modification of our procedure developed for aryl-imido:³⁹ herein, we report a scale-up preparation. A toluene solution (20 mL) of 2.50 g of V(NMe₂)₄ (11.00 mM), 885 mg of ^tBuNH₂ (1.1 equiv, 12.10 mM), and 12.0 g of Me₃SiCl (0.1105 M) was heated overnight at 80 °C upon which time blue needles started to form. The crystallization process was completed by layering the solution with pentane (40 mL). The blue crystals were

collected by decantation, washed with pentane (3×10 mL), and dried under vacuum. Yield of **1a** 2.20 g (71 %). EPR (toluene, 20 °C) $g = 1.985$, $A_{iso}(^{51}V) = 93$ G. μ_{eff} (C₆D₆, Evans) = 1.7 μ_B (300K). Anal. Calcd for C₈H₂₃Cl₂N₃V (MW 283.14): C, 34.94; H, 8.19; N, 14.84. Found: C, 34.88; H, 7.94; N, 14.95.

Synthesis of [V(=N-*t*Bu)Cl₂(Py)₃] (**2a**)

180 mg of [V(=N-*t*Bu)Cl₂(NHMe₂)₂] (**1a**) (0.6357 mM) were dissolved in 2 mL of pyridine. The resulting red solution was slowly layered with, respectively, 2 mL of toluene, and 15 mL of pentane to afford red crystals of **2a**. The crystals were collected and washed with pentane (3×5 mL) and dried under vacuum. Yield: 262 mg (96%). Compound **2a** can also be obtained with similar yield by treating **1a** with 10 equiv of pyridine in dichloromethane. EPR (toluene, 20 °C) $g = 1.990$, $A_{iso}(^{51}V) = 95.7$ G. Anal. Calcd for C₁₉H₂₄Cl₂N₄V (MW 430.27): C, 53.04; H, 5.62; N, 13.02. Found: C, 52.98; H, 5.58; N, 12.94.

Synthesis of [V(=N-CPh₃)Cl₂(NHMe₂)₂] (**1b**)

A dichloromethane solution (5 mL) of 250 mg of V(NMe₂)₄ (1.10 mM), 285 mg of Ph₃CNH₂ (1.10 mM), and 1.20 g of Me₃SiCl (11.05 mM) was stirred at RT for 12 hours. The volatiles were removed under vacuum, and the solid was washed with pentane (3×10 mL), and dried under vacuum to afford 320 mg of yellow solid **1b** (62 %). Large crystals (dark blocks) can be obtained by pentane vapor diffusion into a toluene solution of **1b**. EPR (toluene, 20 °C) $g = 1.987$, $A_{iso}(^{51}V) = 92.6$ G. EPR (CH₂Cl₂, 20 °C) $g = 1.988$, $A_{iso}(^{51}V) = 93.3$ G. μ_{eff} (C₆D₆, Evans) = 1.7 μ_B (300K). Anal. Calcd for C₂₃H₃₉Cl₂N₃V (MW 469.34): C, 58.86; H, 6.23; N, 8.95. Found: C, 58.94; H, 6.24; N, 8.75.

Synthesis of [V(=N-CPh₃)Cl₂(Py)₃] (**2b**)

A dichloromethane solution (3 mL) of 300 mg of [V(=N-CPh₃)Cl₂(NHMe₂)₂] (**1b**) (0.6392 mM) was treated with 870 mg of pyridine (11.0 mM), briefly shaken, and left without stirring for 3 hours upon which time crystallization started to occur. The resulting red solution was slowly layered with, respectively, 3 mL of toluene, and 15 mL of pentane to afford green crystals of **2b**.

The crystals were collected and washed with pentane (3×3 mL) and dried under vacuum. Yield 392 mg (99%). EPR (CH₂Cl₂, 20 °C) $g = 1.985$, $A_{iso}(^{51}\text{V}) = 95.7$ G. Anal. Calcd for C₃₄H₃₀Cl₂N₄V (MW 616.48): C, 66.24; H, 4.91; N, 9.09. Found: C, 66.07; H, 4.97; N, 9.10.

*Synthesis of [V(=N-Ar**)Cl₂(NHMe₂)₂] (1c)*

A toluene solution (3 mL) of 250 mg of V(NMe₂)₄ (1.10 mM), was treated with 506 mg of Ar**NH₂ (1.10 mM), and after 5 min with 1.20 g of Me₃SiCl (11.05 mM), and left at room temperature overnight. The solution turned red with formation of some crystals. The crystallization process was completed by layering the solution with pentane (15 mL). The crystals were collected by decantation, washed with pentane (3×3 mL), and dried under vacuum. Yield of **1c**: 560 mg (76 %). EPR (toluene, 20°C) $g = 1.985$, $A_{iso}(^{51}\text{V}) = 91$ G. EPR (dichloromethane, 20 °C) $g = 1.986$, $A_{iso}(^{51}\text{V}) = 91$ G. μ_{eff} (C₆D₆, Evans) = 1.7 μ_{B} (300K). Anal. Calcd for C₃₆H₃₈Cl₃N₃V (MW 670.01): C, 64.54; H, 5.72; N, 6.27. Found: C, 64.77; H, 5.77; N, 6.19.

*Synthesis of [V(=N-Ar**)Cl₂(Py)₃] (2c)*

A dichloromethane solution (4 mL) of 550 mg of [V(=N-Ar**)Cl₂(NHMe₂)₂] (**1c**) (0.8209 mM) was treated with 870 mg of pyridine (11.0 mM), briefly shaken, and left without stirring for 14 hours upon which time crystallization started to occur. The resulting red solution was slowly layered with, respectively, 6 mL of toluene, and 6 mL of pentane to afford red crystals of **2c**. The crystals were collected and washed with pentane (3×3 mL) and dried under vacuum. Yield: 610 mg (91%). EPR (CH₂Cl₂, 20 °C) $g = 1.985$, $A_{iso}(^{51}\text{V}) = 91$ G. Anal. Calcd for C₄₇H₃₉Cl₃N₄V (MW 817.15): C, 69.08; H, 4.81; N, 6.86. Found: C, 68.99; H, 4.81; N, 6.70.

(Co)polymerization Experiments. General Procedure

Polymerizations were carried out in a 100 mL round-bottomed Schlenk flask containing a stirring bar. Prior to starting polymerization, the reactor was heated to 110 °C under vacuum for 1 h hour and backfilled with nitrogen. The reactor was charged with toluene, the comonomer, ETA and Et₂AlCl in that order, and then brought to the desired polymerization temperature. The solution was degassed and ethylene was added until saturation. The polymerization was started by adding a

toluene solution (2 mg mL⁻¹, dichloromethane for **1a** and **2b**) of vanadium complex via syringe under continuous flow of ethylene. The polymerizations were stopped with methanol containing a small amount of hydrochloric acid; the precipitated polymers were collected by filtration, repeatedly washed with fresh methanol, and finally dried in vacuum at room temperature to constant weight. All the (co)polymerizations were terminated before the amount of formed polymer saturated the solution, and a polymer gel precipitated, and before significant comonomer depletion occurs. These conditions, together with the use of a good solvent, should allow avoiding appreciable effects of the physical status on the copolymerization, and are the key premises for the study of copolymer microstructure.

Characterization

EPR spectra were recorded on a Bruker Elexsys E580 spectrometer. Elemental analysis were performed at the Laboratoire de Chimie de Coordination (Toulouse, France) (C,H,N). Magnetic susceptibility data were measured in solution by ¹H NMR (Evans method).[40] NMR spectra of the obtained (co)polymers were recorded on a Bruker NMR advance 400 Spectrometer operating at 400 MHz (¹H) and 100.58 MHz (¹³C) working in the PFT mode at 103 °C. ¹³C NMR experiments were performed with 10 mm probe in C₂D₂Cl₄ and referred to hexamethyldisiloxane (HMDS) as internal standard. The relaxation delay was 16 s. The molecular weight average (M_w) and the molecular weight distribution (M_w/M_n) were obtained by a high temperature Waters GPCV2000 size exclusion chromatography (SEC) system equipped with a refractometer detector. The experimental conditions consisted of three PL Gel Olexis columns, *ortho*-dichlorobenzene as the mobile phase, 0.8 mL min⁻¹ flow rate, and 145 °C temperature. The calibration of the SEC system was constructed using eighteen narrow M_w/M_n poly(styrene) standards with molar weights ranging from 162 to 5.6×10⁶ g mol⁻¹. For SEC analysis, about 12 mg of polymer was dissolved in 5 mL of *ortho*-dichlorobenzene with 0.05% of BHT as antioxidant. Differential scanning calorimetry (DSC) scans were carried out on a Perkin-Elmer DSC 8000 instrument equipped with a liquid subambient device under nitrogen atmosphere. The sample, typically 5 mg, was placed in a sealed aluminum pan, and the

measurement was carried out from -80 to 130 °C (from -30 to 180 °C for PE homopolymers) using heating and cooling rate of 20 °C min^{-1} . T_m and ΔH_m values were recorded during the second heating. Crystallinity (X) was calculated from the DSC scans as follows: $X = (\Delta H_f / \Delta H_0) \times 100$, where ΔH_f is the enthalpy associated with the melting of the sample and ΔH_0 is the melting enthalpy of a 100% crystalline PE taken equal to 290 J g^{-1} .⁴¹ SSA experiments were performed by DSC following the procedure proposed by Müller.⁴² Preliminary experiments were performed to determine the self-seeding temperature (T_s), *i.e.*, the lowest temperature of domain II. SSA temperature program was set as follows: the copolymer was first held in the melt at 130 °C for 3 min and cooled to -40 °C at a rate of 10 °C min^{-1} to create the initial standard state. Then, the copolymer was heated to the selected T_s , at a rate of 10 °C min^{-1} , and held at this temperature for 5 min. After that, the sample was cooled from T_s to -40 °C, heated to the second T_s which was 5 °C lower than the previous T_s , and held in isothermal condition for 5 min. This cyclic procedure was repeated several times, using heating and cooling rates of 10 °C min^{-1} , and a fractionation window equal to 5 °C. Finally, the copolymer was heated from chosen minimum temperature up to 130 °C. Thermogravimetric analysis (TGA) was performed on a Perkin–Elmer TGA-7 instrument under a nitrogen atmosphere. Before performing the TGA run, the sample (2.5 mg) was held at 50 °C for 30 min; the scan was carried out from 50 to 750 °C at a heating rate of 20 °C min^{-1} . The materials for the mechanical characterization were molded in a press at 110 – 125 °C, and 50 bar for 5 min, then the press plates were cooled to 20 °C min^{-1} to room temperature. Films with a thickness of about 120 μm were produced. Tensile dog-bone-shaped specimens (length overall 75 mm, gauge length 25 mm, and width of narrow section 4 mm) were analyzed at 20 °C using a Zwick Roell ProLine Z010 mechanical tester equipped with a XforceP (50 N) load cell at a constant crosshead rate of 15 mm/min. For each material, at least five samples were tested. In the recovery experiment performed at 300% strains, the specimens were cyclically loaded and unloaded in uniaxial tension.

Single crystal X-ray diffraction determination

Crystals suitable for X-ray structure determination were obtained for compounds **Ar**NH₂**, **1a–c**, and **2c** (generally by diffusion of pentane into a toluene solution of the complexes). The crystals were kept in the mother liquor until they were dipped into perfluoropolyether oil and their structure was determined. Crystal data collection and processing parameters are given in Supplementary Materials.

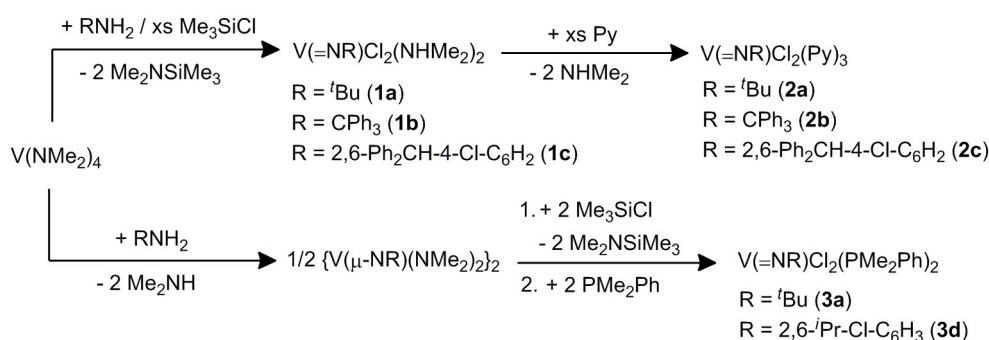
The chosen crystals were mounted on a Mitegen micromount and quickly cooled down to 180 K. The selected crystals of **Ar**NH₂** (pale yellow block, 0.15 × 0.10 × 0.05 mm³), **1a** (blue, 0.23 × 0.15 × 0.08 mm³), **1b** (orange stick, 0.10 × 0.15 × 0.35 mm³), **1c** (orange plate, 0.18 × 0.10 × 0.03 mm³), and **2c** (red plate, 0.15 × 0.10 × 0.02 mm³), were mounted respectively on a Bruker Kappa APEX II (**Ar**NH₂**, **1c**, **2c**), Oxford Diffraction Xcalibur (**1a–b**) diffractometers, using molybdenum ($\lambda = 0.71073 \text{ \AA}$) and equipped with an Oxford Cryosystems cooler device or an Oxford Cryosystems Cryostream Cooler Device. The unit cell determination and data integration were carried out using CrysAlis RED package or APEX II.^{43–45} The structures have been solved by Direct Methods using SIR92,⁴⁶ and refined by least-squares procedures with SHELXS-2016⁴⁷ included in the software packages WinGX version 1.63.⁴⁸ Atomic Scattering Factors were taken from the International tables for X-Ray Crystallography.⁴⁹ All hydrogen atoms were refined by using a riding model. All non-hydrogen atoms were anisotropically refined. Drawings of molecules have been performed with the program Ortep-3 for Windows.⁵⁰ Details of the structure solution and refinements are given in the Supplementary Materials, together with a full listing of atomic coordinates, bond lengths and angles, and displacement parameters for all structures. These data have also been deposited at the Cambridge Crystallographic Data Centre. CCDC 1940732–1940736 contains the supplementary crystallographic data for this paper. These data can be obtained free of charge from The Cambridge Crystallographic Data Centre via www.ccdc.cam.ac.uk/data_request/cif.

RESULTS AND DISCUSSION

Preparation and characterization of the complexes

The imido pre-catalysts $V(=NR)Cl_2(L)_n$ ($R = tBu, CPh_3, 2,6-CHPh_2-4-Cl-C_6H_2, 2,6-iPr_2-C_6H_3$; $n = 2$: $L = NHMe_2$ and $L = PMe_2Ph$; $n = 3$: $L = Py$) were prepared according to our previously reported synthesis for making similar Ti and V complexes.³⁹ The general synthetic pathways are depicted in Scheme 1. In the following, the complexes are named referring to their structure: the number identifies the coligand (**1** stands for $NHMe_2$, **2** for Py , and **3** for $PPhMe_2$), while the letter identifies the R substituent in imido ligand [$R = tBu$ (**a**), $R = CPh_3$ (**b**), $R = 2,6-CHPh_2-4-Cl-C_6H_2$ (**c**), and $R = 2,6-iPr_2-C_6H_3$ (**d**)].

Scheme 1. Synthetic pathways leading to $V(=NR)Cl_2(L)_n$ complexes [$L = NHMe_2, Py, PMe_2Ph$; $R = tBu, CPh_3, 2,6-CHPh_2-4-Cl-C_6H_2, 2,6-iPr_2-C_6H_3$].



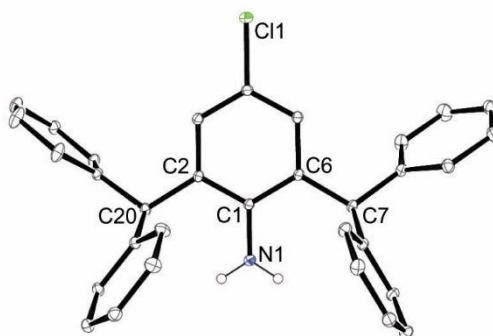
The pyridine adducts are obtained from the transamination reaction of $V(NMe_2)_4$ with a primary amine, immediately followed by chlorination with trimethylchlorosilane (in a one-pot reaction), *via* the intermediacy of the bis-dimethylamine adducts **1**. The bis-dimethylamine adducts are further converted into the desired pyridine complexes **2** by treatment with excess pyridine. The phosphine adducts are produced from a similar reaction of $V(NMe_2)_4$ with a primary amine, but the dimethylamines produced need to be removed prior to addition of trimethylchlorosilane. Treating the bridging imido-amido intermediate with Me_3SiCl , affords ill-defined oligomeric or polymeric complexes,^{39,51-54} that upon treatment with phosphine give the phosphine adducts **3**.^{35,37,55}

All these V(IV) complexes are NMR silent ($^1H, ^{51}V$) but EPR active (Figure S1–S6) due to their d^1 configuration ($\mu_{eff} = 1.7 \mu_B$). They present an 8-line pattern in their EPR spectra in an

analogous way to previously reported examples of imido-V(IV) complexes ($I = 7/2$ for ^{51}V) with $g_{iso} = ca. 1.98$, and $A_{iso}(^{51}\text{V}) = ca. 90\text{--}95\text{G}$.

Single crystal structure determination of some of these complexes was used to compare the steric and electronic properties of the imido ligand in $\text{V}(=\text{NR})\text{Cl}_2(\text{L})_n$ complexes in order to correlate with their catalytic properties (*vide infra*). Although it will not be discussed in the article, we also determined the structure of the bulky aniline 2,6-*CHPh*₂-4-Cl-C₆H₂NH₂ (Figure 1), employed for the synthesis of **1c** and **2c**.

Figure 1. Molecular structure of **Ar**NH₂**. Thermal ellipsoids are drawn at the 50% probability level and partial atom-labeling schemes. Hydrogen atoms are omitted for clarity (except for H atoms on N).



Crystals suitable for molecular structure determination were obtained for **1a**, **1b** and **1c**, which allow a direct comparison with the known structure of $[\text{V}(=\text{N}-2,6\text{-}i\text{Pr}_2\text{-C}_6\text{H}_3)\text{Cl}_2(\text{NHMe}_2)_2]$ (**1d**).³⁹ ORTEP drawings of the molecules of **1a**, **1b** and **1c** are displayed in Figure 2, 3 and 4, respectively, and important metric parameters (interatomic bond distances and angles) are given in Table 1 for that purpose together with those of **1d**.

Figure 2. Molecular structure of **1a**. Thermal ellipsoids are drawn at the 50% probability level and partial atom-labeling schemes. Hydrogen atoms are omitted for clarity (except for H atoms on N). View Article Online
DOI: 10.1039/C9PY01415B

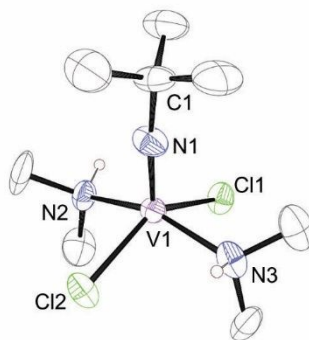


Figure 3. Molecular structure of **1b**. Thermal ellipsoids are drawn at the 50% probability level and partial atom-labeling schemes. Hydrogen atoms are omitted for clarity (except for H atoms on N).

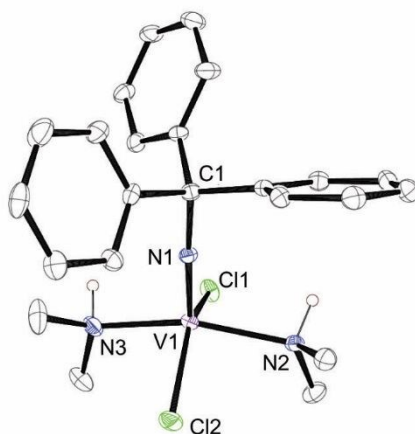
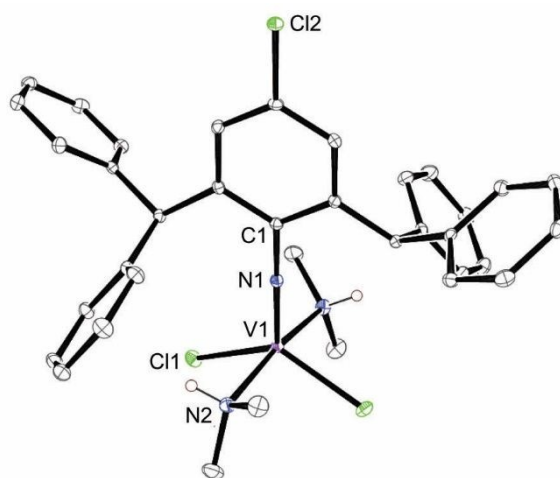


Figure 4. Molecular structure of **1c**. Thermal ellipsoids are drawn at the 50% probability level and partial atom-labeling schemes. Hydrogen atoms are omitted for clarity (except for H atoms on N).



Dimethylamine adducts **1a**, **1b** and **1c** share similar structural features, in agreement with their known parent **1d**. The pentacoordinate vanadium center has a geometry between a distorted

trigonal-bipyramid (with equatorial aryl-imido and chlorine atoms) and a square pyramid (with the imido group in apical position) as reflected by the measure of the τ parameter ($\tau = 0.29\text{--}0.64$).⁵⁶ The salient bond parameters are typical of such imido complexes: a short V–N bond distance of *ca.* 1.64–1.67 Å with almost linear V–N–C imido linkage, two mutually *trans* dimethylamino ligands [NH–V–NH = 158–170° with V–NH distances of *ca.* 2.15 Å], and two mutually *cis* chlorine atoms [mean V–Cl bonds of *ca.* 2.30–2.35 Å, Cl–V–Cl angle = *ca.* 135°].

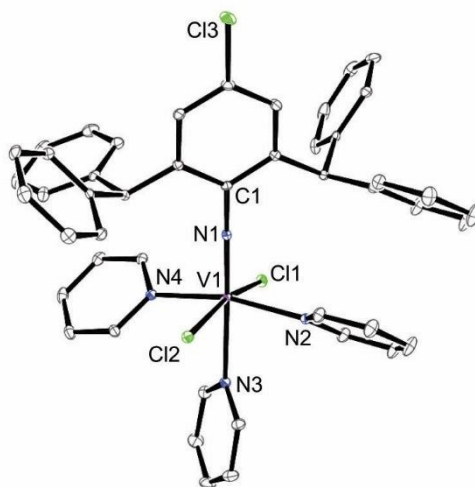
Table 1. Comparison of Average Interatomic Distances (Å) and Angles (deg) in **1a–1d**.

	1a	1b^a	1c	1d^b
V–N _{imido}	1.636(4)	1.639(3)	1.6705(15)	1.654(3)
N–C	1.473(6)	1.476(4)	1.379(2)	1.380(5)
V–Cl	2.346(3)	2.3381(11) (Cl1)	2.3012(3)	2.3199(14) (Cl1)
	2.338(9)	2.3150(11) (Cl2)		2.3268(12) (Cl2)
V–N _{NHMe2}	2.173(9) (N2)	2.175(3) (N2)	2.1681(11)	2.007(5) (N2)
	2.129(10) (N3)	2.110(4) (N3)		2.162(4) (N3)
V–N _{imido} –C	172.30(10)	177.1(3)	180	178.4(3)
Cl–V–Cl	140.56(5)	139.19(5)	131.58(2)	136.48(5)
NH–V–NH	158.05(16)	160.39(12)	169.95(6)	165.17(16)
τ^c	0.29	0.35	0.64	0.48

^a Data only for molecule *A* (two independent molecules in the cell). ^b Data from ref. 57; ^c τ is the angular parameter commonly used to describe the geometry around the metal center in pentacoordinate complexes, and defined as $\tau = (\alpha - \beta)/60$ (α and β are the two largest L–M–L bond angles, with $\alpha \geq \beta$, see ref. 56).

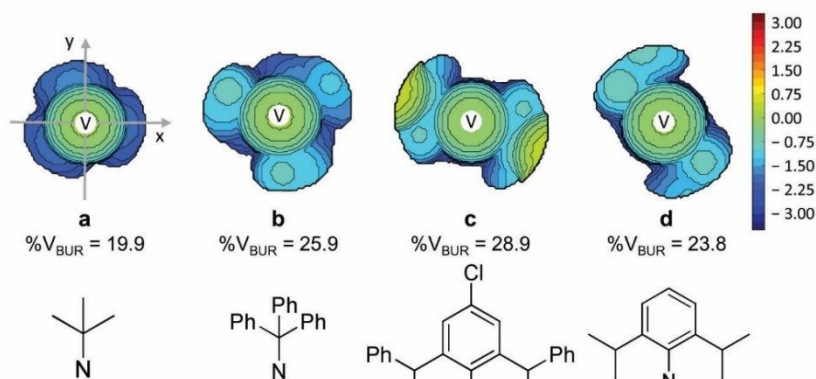
Crystals suitable for molecular structure determination were also obtained for **2c**. An ORTEP drawing of the molecule of **2c** is shown in Figure 5. The complex has a pseudo-octahedral geometry with mutually *trans* chloride and pyridine ligands, and with a third pyridine ligand being *trans* to the imido group. Bond parameters are found very similar to the known V(=N-2,6-*i*Pr₂-C₆H₃)Cl₂(Py)₃: [39] the V–N_{imido} bond distance of the imido fragment is 1.6847(17) Å, V–N_{imido}–C of 171.54(15)°, and average V–Cl of 2.324(4) Å. The mutually *trans* V–N_{py} of 2.1740(18) Å and 2.1631(18) Å are significantly shorter than the third V–N_{py} bond distance of 2.3184(18) Å due to the *trans*-labilizing ability of the imido function.

Figure 5. Molecular structure of **2c**. Thermal ellipsoids are drawn at the 50% probability level and partial atom-labeling schemes. Hydrogen atoms are omitted for clarity.



We attempted to make a rough classification of imido ligands based on their electronic and steric properties. Considering the electronic properties of the substituents on the imido moiety, the electron donor ability should increase in the order $2,6\text{-CHPh}_2\text{-4-Cl-C}_6\text{H}_2 < 2,6\text{-}^i\text{Pr}_2\text{-C}_6\text{H}_3 < \text{CPh}_3 < ^t\text{Bu}$. The steric properties of the imido ligands were rationalized on the basis of X-ray structural data for complexes **1a–d**, and by the use of SambVca 2 Web.^{58,59} The $\%V_{\text{BUR}}$ and the topographic steric maps of imido ligands **a–d** are reported in Figure 6 (full details are given in Figure S7–S10). Although it is difficult to compare ligands that have a more planar hindrance (*i.e.*, aryl-imido) with others that have bulky groups in all the three dimensions (*i.e.*, ^tBu , CPh_3), according to this study we could suggest the following order for the steric demand of the imido function: $^t\text{Bu} < 2,6\text{-}^i\text{Pr}_2\text{-C}_6\text{H}_3 < \text{CPh}_3 < 2,6\text{-CHPh}_2\text{-4-Cl-C}_6\text{H}_2$.

Figure 6. Topographical ligand steric maps and percent buried volume ($\%V_{\text{BUR}}$) of **a–d**.

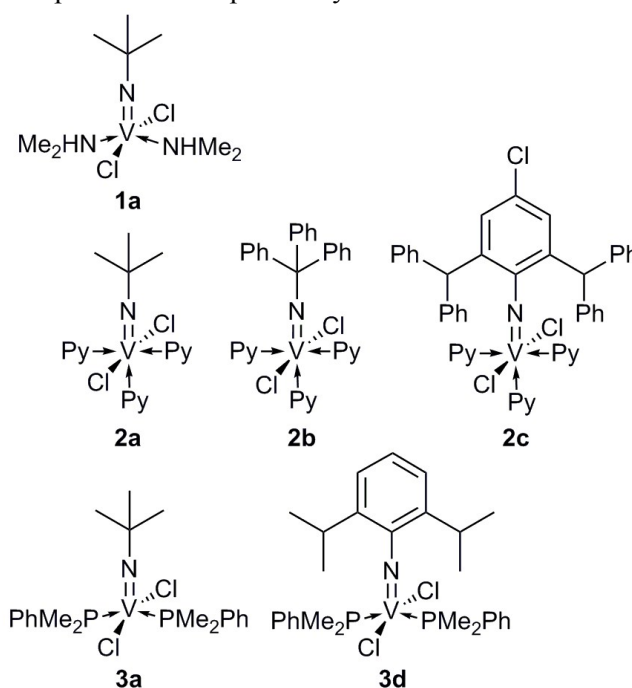


Polymerization

View Article Online
DOI: 10.1039/C9PY01415B

Compounds **1a**, **2a–c**, **3a** and **3d** (Scheme 2), in combination with Et_2AlCl and ETA, were first selected as catalysts for the polymerization of ethylene. The polymerizations were carried out under the same set of conditions using 500 equiv. of Et_2AlCl and 10 equiv. of ETA, at an ethylene pressure of 1 atm, and in toluene (Table 2). We chose the chloroalkylaluminum in place of methylaluminoxane (MAO) as cocatalyst because we recently demonstrated that Et_2AlCl was beneficial to obtain at least one order of magnitude higher catalytic activities with **3a** and **3d**.³⁵ The polymerizations were performed in the presence of ETA, which acts as reoxidant, limiting the spontaneous deactivation of vanadium complexes associated with the faster reduction to low-valent, less active V(II) species.⁶⁰

Scheme 2. $\text{V}(=\text{NR})\text{Cl}_2(\text{L})_n$ complexes used as pre-catalyst in this work.



Except the bis-dimethylamine **1a**, pyridine and PMe_2Ph complexes (**2** and **3**, respectively) were instantaneously activated. The polymerization occurred so fast that the solution viscosity increased within the first seconds of reaction. To avoid mass transport limitations caused by filling of the reactor with the swollen polymer, the polymerizations were stopped rapidly. The productivity does not change significantly moving from phosphine **3** to pyridine **2** complexes, although steric

and electronic properties of imido fragment were deeply altered. Changes in the imido ligand substitution brought no significant effect on the polymerization course and on the catalytic activity under the conditions employed.

Table 2. Polymerization of ethylene and copolymerization with propylene catalyzed by (imido)V(IV) complexes in combination with Et₂AlCl and ETA.^a

entry	complex	P/E ^b	time (min)	yield (mg)	activity ^c	P ^d (mol%)	M _w ^e (×10 ³)	M _w /M _n ^e	T _m ^f (°C)	ΔH _m ^f (J/mol)	regioirreg. ^g (%)
1	1a		1	traces							
2	1a		4	82	490		410	2.3	138		
3	2a		1	80	1920		370	2.1	137		
4	2b		1	90	2260		300	2.1	138		
5	2c		1	75	1740		280	2.1	138		
6	3a		1	100	2470		290	2.1	139		
7	3d		1	94	2260		310	2.1	137		
8	1a	4	3	100	400	4.2	270	2.1	115	113	nd ^h
9	2a	4	2	270	1630	9.7	170	2.3	94 (82) ⁱ	72	6.1
10	2a	4	4	700	2100	13.7	98	2.7	62 (89)	55	8.7
11	2c	4	1'30"	230	1840	8.9	140	2.2	98 (84)	80	6.5
12	3a	4	2	270	1620	9.2	160	2.2	85 (93)	76	6.1
13	3d	4	1'30"	246	1970	7.8	165	2.2	105 (92)	94	5.7
14 ^l	3d	3	5	560	1350	12.4	240	2.2	81 (94)	63	6.1

^a polymerization conditions: ethylene pressure, 1.01 bar; total volume, 50 mL (toluene); V complex, 2.5 μmol for ethylene polymerizations, and 5 μmol for ethylene/propylene copolymerizations; Al/V = 500; ETA/V = 10; temperature, 20 °C; ^b P/E feed ratio (mol/mol) in liquid phase; ^c activity in kg_{pol}×(mol_V×h)⁻¹; ^d determined by ¹H NMR; ^e determined by SEC; ^f determined by DSC; ^g regioirregularities calculated according to Randall as [100(½S_{αβ} + ½S_{βγ})/(S_{αα} + ½S_{αβ} + S_{ββ} + ½S_{βγ} + S_{γγ} + ½S_{γδ})] from ¹³C NMR;⁶¹ ^h not determined because the sample is rather insoluble in C₂D₂Cl₄; ⁱ in parenthesis the minor melting peak; ^l temperature, 0 °C; total volume, 25 mL (toluene).

Solid PEs with high molecular weight (M_w from 280 to 410 ×10³ g mol⁻¹), and narrow, unimodal molecular weight distributions (M_w/M_n ca. 2) were obtained. The PEs are linear polymers, with melting temperatures (T_m) in the range from 137 to 139 °C, and crystallinity of about 70% (ΔH_m ca. 200 J mol⁻¹) (Figure S11). In the case of pyridine **2a–2c**, in which steric and electronic properties of imido ligand were deeply changed, the molecular weight of the obtained PEs increased in the order **2c** ($M_w = 280000$ g mol⁻¹, entry **5**) < **2b** ($M_w = 300000$, entry **4**) < **2a** ($M_w = 370000$, entry **3**). This trend may be because the electron-donating *tert*-butyl imido group for **2a** strengthens the V–N bond, improving the stability of the electron-deficient catalytic intermediate, and reducing

the chain-transfer rate. An analogous trend was already observed with phosphine (imido)vanadium complexes.³⁵

None of the (imido)vanadium complexes catalyze the homopolymerization of propylene. We have never recovered solid polymer either in experiment with liquid propylene or with the gaseous monomer at atmospheric pressure. This could be likely due to a high propensity of the investigated vanadium complexes to undergo faster chain-transfer, and subsequent chain-termination in the presence of propylene.

The performance of selected **1a**, **2a**, **2c**, **3a**, and **3d** was then explored in the copolymerization of ethylene with propylene. The results are listed in Table 2. Copolymerizations were performed at P/E = 4 in a semibatch mode: the ethylene gaseous monomer was replenished by maintaining a constant gas pressure during the reaction timecourse, while all the liquid propylene was placed in the reactor at the beginning of the reaction. To avoid undesirable compositional drifting and copolymer inhomogeneity, due to the high initial efficiency and faster consumption of the most reactive comonomer, the copolymerization was quenched before significant comonomer depletion occurs. By controlling the propylene conversion, and keeping it at low level ($\leq 5\%$), the variation of the propylene feedstock concentration can be considered negligible, and the relative comonomer concentration can be considered constant, to the greatest possible extent.

With the exception of dimethylamine **1a**, that as in the case of the homopolymerization of ethylene exhibits a much lower activity, particularly at the first stage (Table 2, entry **8**, $404 \text{ kg}_{\text{pol}} \text{ mol}_v^{-1} \text{ h}^{-1}$, P = 4.2 mol%), pyridine and PMe_2Ph complexes were instantaneously activated and good activities, in the range from 1620 to $2100 \text{ kg}_{\text{pol}} \text{ mol}_v^{-1} \text{ h}^{-1}$, were obtained. The resulting copolymers have a propylene content from 7.8 to 13.7 mol%, reasonably narrow molecular weight distribution ($2.1 < M_w/M_n < 2.7$), and molecular weight lower than those of PEs, indicating the increased rate of chain-termination in the presence of propylene: the higher the content of propylene, the lower the copolymer molecular weight. A copolymer with a molecular weight as

high as $240000 \text{ g mol}^{-1}$ was obtained at subambient temperature, that restrains the chain-transfer to some extent (Table 2, entry **14**, P = 12.4 mol%).³⁵

The pyridine or PMe_2Ph coligands have a limited effect on the catalytic activity, copolymer composition, and molecular weight, at least under the experimental conditions employed (Table 2, entry **9** vs **12**). We attribute this result to the fact that the space around the catalytic active is not so congested, probably because the coligands move further apart from the centers. In contrast, the reason why dimethylamine **1a** exhibits lower activity compared to **2a** and **3a**, all bearing the same *tert*-butyl imido fragment, is not clear at this stage. A possible hypothesis can be derived from electronic coligand properties: the Lewis base character of the investigated coligands increases in the order $\text{PMe}_2\text{Ph} \approx \text{Py} < \text{NHMe}_2$. Since the active V-center has a partial positive charge (δ^+), it may be inferred that NHMe_2 , having the more Lewis base character, will remain more close to the active center, thus limiting the approach of the monomer, and slowing down the polymerization rate. Another possible explanation is the involvement of a probable deleterious interaction between the amine and the aluminum alkyl, leading to the deprotonation of NHMe_2 .⁵²

Changes in the imido ligand substitution have an effect on the course of E/P copolymerization. Copolymerizations with **2c** and **3d**, having more electron-withdrawing aryl-imido substituents (Table 2, entry **11** and **13**, respectively), are faster than those with **2a** and **3a**, with more electron-donating *t*Bu imido (Table 2, entry **9** and **12**). The highest initiation rate of **2c** and **3d** results in high medium copolymerization viscosity, so that shorter time is required to reach good productivity and restrict diffusional comonomers mobility to guarantee desired and comparable reaction homogeneity. In this respect, electronic ligand effects play a key role. Indeed, **2c** and **3d** may have a pronounced preference to accept electron density from the (co)monomers, at least at the initial polymerization stage. This faster monomer insertion may explain the enhanced initiation rate of **2c** and **3d**. The same trend was recently found by us in the copolymerization of ethylene with cyclic olefins, particularly in the case of 5-ethylene-2-norbornene, and dicyclopentadiene.³⁵

As anticipated, the obtained copolymers have a moderate propylene content (from 7.8 to 13.7 mol%). Although it is difficult to make a comparison with the literature due the different operating conditions (batch *vs* semibatch) and objectives, the amount of propylene incorporated in the copolymers with the vanadium complexes under investigation is comparable to the same data for vanadyl C- and N-capped tris(phenolate) complexes,⁶² V(V) tetra-phenolate complexes,⁶³ and vanadyl calix[6]arene one,⁶⁴ but lower than *N*-heterocyclic carbenes,^{34,65} naphthalene-bridged nitrogen-sulfonate ligands,⁶⁶ and amide V(IV) complexes.⁶⁷

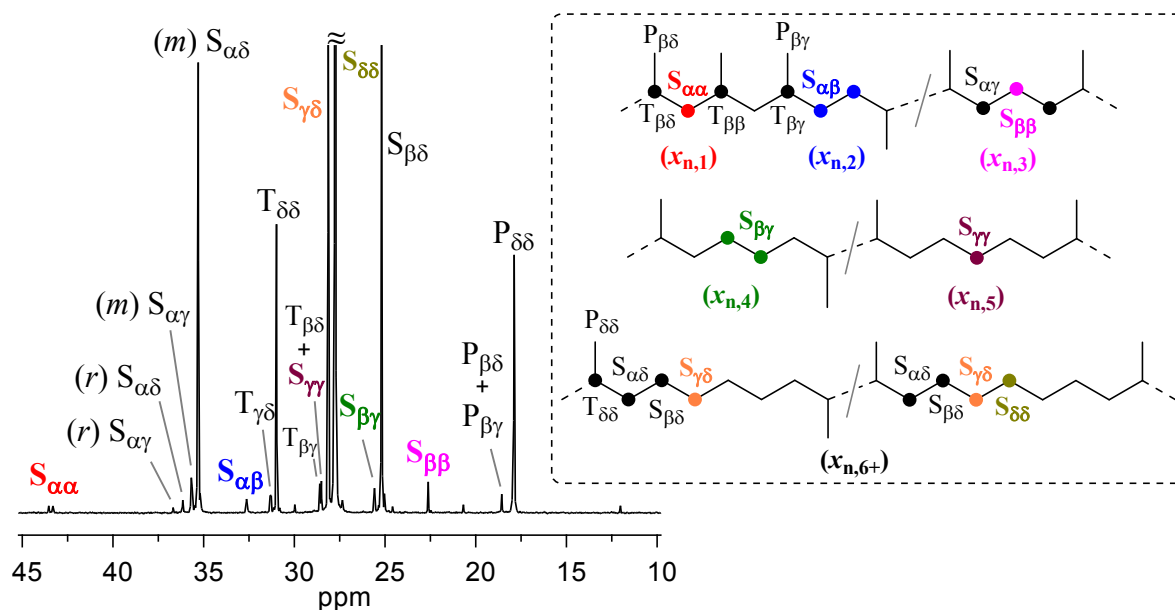
Copolymers Composition

The poly(ethylene-*co*-propylene)s microstructure was investigated by ¹³C NMR (Figure 7). The resonance peaks were assigned according to the literature, and followed the terminology used by Carman et al,⁶⁸ where primary (methyl), secondary (methylene) and tertiary (methine) carbons were denoted as P, S, and T, respectively. The position of a carbon atom relative to its nearest methine was labeled by two Greek subscripts.

In addition to the characteristic peaks of isolated and alternating propylene units spanning long methylene segments, the spectra is complicated by the presence of several resonances, which are diagnostic of stereoirregular and regioirregular propylene homosequences, and propylene units. Calculation of propylene inversion, *i.e.*, 2,1-insertion, reveals that the copolymers have regioirregularities in the range from 5.7 to 8.7% (Table 2). The presence of regioirregularities in the propylene placement complicates the description of the copolymer microstructure, and precludes a quantitative evaluation of the comonomer distribution at triad level by ¹³C NMR: single succession of ethylene and propylene units such as PEP, and EPP cannot describe the unique carbon sequence in the case under investigation. Similarly, the determination of the reactivity ratio through the classical Finemann and Ross method may be inaccurate and unreliable. To avoid problems associated with propylene inversion, a direct ¹³C NMR quantitative method,^{61,69} was used to give a description of the copolymer microstructure. This method, first developed by Randall,⁶¹ aims to distinguish the copolymers on the basis of uninterrupted methylene sequence distribution from one

to six and longer. Specifically, the number fraction ($x_{n,i}$) of uninterrupted methylene sequence of length i , the total number fraction of even methylene sequences ($\sum x_{n,2i}$), generated by propylene inversion, the number-average sequence length of uninterrupted methylene carbons (n_0), and that of uninterrupted sequences of two or more methylene carbons (n_{2+}) is calculated (Table 3).

Figure 7. ^{13}C NMR spectrum (in $\text{C}_2\text{D}_2\text{Cl}_4$ at 103 °C, reference to HDMS) of a selected poly(ethylene-*co*-propylene) (Table 2, entry 10, P = 13.7 mol%).



In addition, from uninterrupted methylene sequences, the chain propagation probability for ethylene to insert at the last inserted ethylene unit (P_{EE}) was calculated according to ref. 70. The application of this method is possible because each isolated 2,1-insertion of propylene gives a unique direction to the growing macromolecular chain, thus making possible to describe the monomer sequencing in the immediate vicinity of each isolated 2,1-insertion. Methylene segments are uniquely identified by resonances $S_{\alpha\alpha}$, $S_{\alpha\beta}$, $S_{\beta\beta}$, $S_{\beta\gamma}$ and $S_{\gamma\gamma}$ for one ($x_{n,1}$), two ($x_{n,2}$), three ($x_{n,3}$), four ($x_{n,4}$), and five ($x_{n,5}$) uninterrupted methylene sequence, respectively, while those sequences of six and longer methylene ($x_{n,6+}$) give both $S_{\gamma\delta}$ and $S_{\delta\delta}$ resonances (Figure 7). It is worth noting that, since $S_{\gamma\gamma}$ overlaps with $T_{\beta\delta}$, the former can be calculated as $0.5 \times (S_{\beta\delta} - S_{\gamma\delta})$.

In general, n_0 and n_{2+} are strongly affected by the copolymer composition, with lower values by increasing the content of propylene. The $x_{n,6+}$ dominates the distribution, thus reflecting the

tendency toward a blocky sequence of ethylene. Sample **14**, obtained at subambient temperature, exhibits the highest concentration of $x_{n,1}$: the copolymer has a more blocky propylene units, most likely due to the lower solubility of ethylene with decreasing the copolymerization temperature.

Table 3. The Number Fractions of Uninterrupted Methylene Sequences and Average Sequence Lengths for Ethylene-*co*-Propylene Copolymers.

entry	complex	P ^a (mol%)	$x_{n,1}^b$	$x_{n,2}^b$	$x_{n,3}^b$	$x_{n,4}^b$	$x_{n,5}^b$	$x_{n,6+}^b$	$\Sigma x_{n,2i}^c$	n_0^d	n_{2+}^e	P_{EE}^f
9	2a	9.7	0.037	0.027	0.070	0.034	0.024	0.807	0.354	19.7	20.5	0.35
10	2a	13.7	0.053	0.045	0.118	0.043	0.080	0.661	0.297	13.3	14.0	0.68
11	2c	8.9	0.022	0.028	0.074	0.037	0.033	0.807	0.378	21.0	21.5	0.44
12	3a	9.2	0.050	0.033	0.072	0.028	0.018	0.799	0.323	19.2	20.1	0.25
13	3d	7.8	0.028	0.029	0.058	0.028	0.019	0.838	0.382	24.8	25.5	0.32
14	3d	12.4	0.129	0.028	0.088	0.032	0.039	0.684	0.231	15.3	17.4	0.44

^a propylene molar fraction in the copolymer determined by NMR; ^b $x_{n,i}$, the number fraction of uninterrupted methylene sequence of length i ; ^c the total number fraction of even methylene sequences; ^d the number-average sequence length of uninterrupted methylene carbons; ^e the number-average sequence length of uninterrupted sequences of two or more methylene carbons; ^f the chain propagation probability for ethylene to insert after a last ethylene inserted unit.

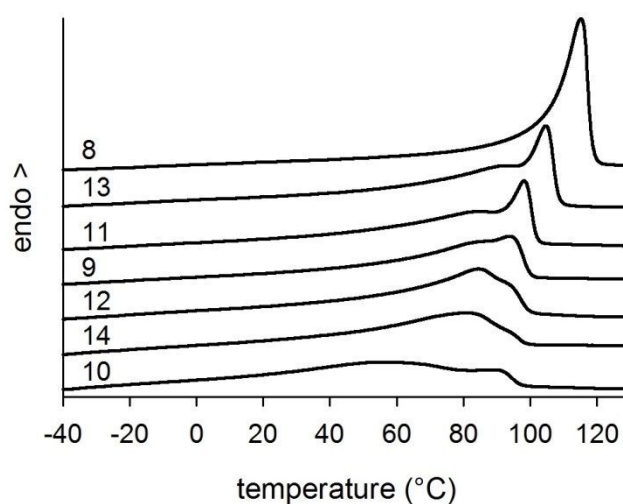
Sample **11** and **13** (from **2c** and **3d**, respectively) have a higher fraction of $\Sigma x_{n,2i}$ (generated by propylene inversion) with respect to sample **9**, **10**, and **12** (from **2a** and **3a**). This could be likely due to the higher steric hindrance around the metal in **2c** and **3d** compared to the ^tBu-imido in **2a** and **3a** (Figure 6), and the concomitant differing steric demand of secondary insertion than a primary insertion. Indeed, it is known that a 2,1-insertion of propylene places the methyl in a peripheral position (rather than in the direction or plane of the metal), and the resultant intermediate transition state requires less space along the direction of metal aperture to undergo a 2,1-insertion.^{10,71} It is worth noting that $\Sigma x_{n,2i}$ only indicates the minimum fraction of inverted propylene units since the calculated data neglects all the inverted units contained in the methylene sequences longer than six methylene units (n_{6+}), and 1,3-enchaind propylene units arising from a 2,1→1,3 isomerization.

Thermal Properties

The DSC heating curves of non-isothermal crystallized poly(ethylene-*co*-propylene)s are reported in Figure 8. The overall melting event of the copolymers occurs at a lower temperature range than that of pure PE (Figure S11) and, in general, it decreases with the increase of the

comonomer content as expected for random copolymers (T_m and ΔH_m in Table 2). **Sample 8** with the lowest content of comonomer ($P = 4.2$ mol%) shows a single (and relatively sharp) endothermic transition with melting peak at 115 °C, and crystallinity of 39%. Increasing the propylene content, the copolymers exhibit a broader and multimodal melting endotherm due to the non-homogeneous distribution of crystallizable units along the polymer chain, and among the polymer chains (*i.e.*, intra- and inter-molecular heterogeneity). In general, the peak at low temperature relates to the macromolecular chain segments with a low content of crystallizable sequences, whereas the peak at higher temperature to segments with longer crystallizable sequences.

Figure 8. DSC heating scans of ethylene-*co*-propylene copolymers (Table 2).



It is worth noting that copolymers with a comparable content of propylene ($7.8 < P$ mol% < 9.7) show different thermal behavior, *i.e.*, DSC profiles, T_m and ΔH_m values (Table 2, entry **9**, **11**, **12**, and **13**). However, standard DSC technique does not allow the appreciation of subtle microstructural differences; for this reason these four copolymers were characterized by SSA to reveal detailed changes in the crystallizable sequence length and lamellae thickness.

Figure 9 shows the final heating scans after the SSA procedure, displaying the melting of all the fractions created for the copolymers obtained with different catalyst. In general, the SSA final scan of copolymers exhibits several narrow peaks spread along the temperature axis and the profile

results to be different from the broad endothermic transition registered by standard DSC heating run. The SSA thermograms show marked differences in the peaks positions, and in the peaks enthalpy. The variation in the number and magnitude of melting peaks can be attributed to the difference of the crystalline sequence length distribution. The lamellar thickness (l), the methylene sequence length (MSL) and relative polydispersities (D) were determined from final SSA thermograms, according to the literature (Table 4).⁷²⁻⁷⁵

Figure 9. Final melting curves obtained after SSA thermal fractionation of selected ethylene-*co*-propylene copolymers: (a) entry **13**, (b) entry **11**, (c) entry **9**, and (d) entry **12**.

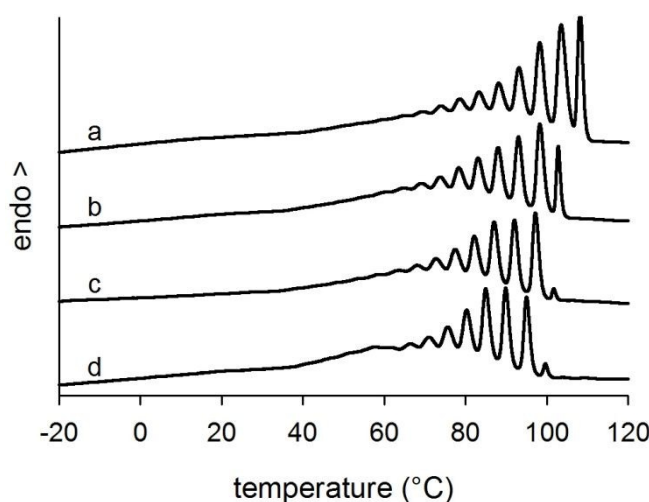


Table 4. Self-nucleation temperature (T_s) and SSA data of selected poly(ethylene-*co*-propylene)s.

entry	complex	P ^a (mol%)	T_s	l_w^b (nm)	l_n^b (nm)	D_l	MSL_w^c	MSL_n^c	D_{MSL}
9	2a	9.7	102	5.7	5.4	1.1	41	39	1.1
11	2c	8.9	103	5.8	5.4	1.1	45	41	1.1
12	3a	9.2	105	5.4	5.1	1.0	40	38	1.0
13	3d	7.8	108	6.8	6.2	1.1	54	48	1.1

^a propylene molar fraction in the copolymer determined by NMR; ^b lamellar thickness; ^c methylene sequence length.

The copolymer from **3d** (entry **13**) presents the thickest lamellae, and the longest methylene sequence, while the sample obtained from **3a** (entry **12**) shows the thinnest lamellae, and the shortest methylene sequence. MSL data calculated from SSA are slightly higher than the number-average sequence length of uninterrupted methylene carbons determined by ¹H NMR (n_o in Table 3), but the same trend was obtained by means of both techniques.

Copolymerization of ethylene with higher α -olefins

We performed some preliminary copolymerizations of ethylene with 1-octene by using **2a**, **3a** and **2c**, and with 1-hexene and 4-methyl-1-pentene with the best performing **2a**. The results are summarized in Table 5.

Table 5. Copolymerization of ethylene with α -olefin (Y) catalyzed by selected (imido)V(IV) complexes in combination with Et₂AlCl and ETA.^a

entry	complex	Y (type)	time (min)	yield (mg)	activity ^b	Y ^c (mol%)	M _w ^d (×10 ³)	M _w /M _n ^d	T _m ^e (°C)	ΔH ^e (J/mol)
15	2a	OCT	4	390	1160	9.0	64	2.3	85	58
16	2c	OCT	4	280	840	6.7	79	2.1	91	71
17	3a	OCT	2	160	940	6.5	97	2.6	93	75
18	2a	HEX	4	560	1680	11.2	69	2.3	86 (70) ^f	61
19	2a	4M1P	4	220	660	4.7	55	2.3	104 (110)	90
20	2a	4M1P	6	390	1170	5.1	36	2.2	101	84

^a polymerization conditions: ethylene pressure, 1.01 bar; total volume, 50 mL (toluene); V complex, 5 μmol; Al/V = 500; ETA/V = 10; temperature, 20 °C; Y/E = 4, feed ratio (mol/mol) in liquid phase; ^b activity in kg_{pol} × (mol_V × h)⁻¹; ^c determined by NMR; ^d determined by SEC; ^e determined by DSC; ^f in parenthesis the minor melting peak.

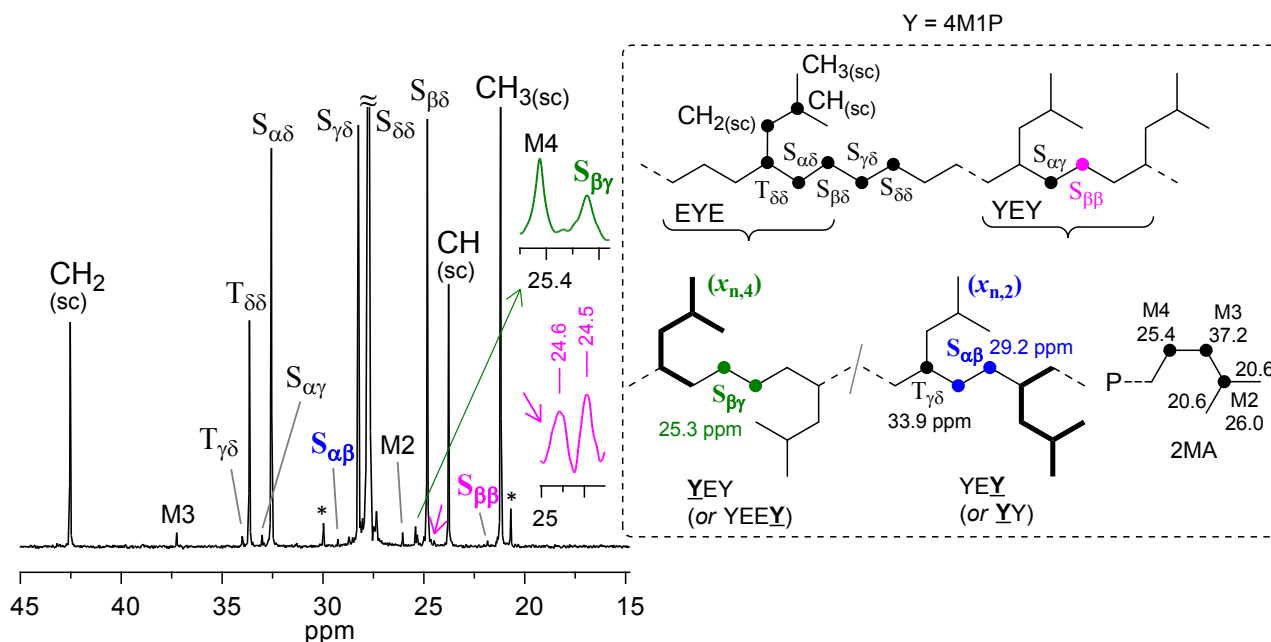
The copolymerization of ethylene with 1-octene proceeds with moderate activities. Generally, the resulting activities are lower than those for the copolymerization of ethylene with propylene, most likely due to the increased steric interaction in the case of 1-octene. The copolymerization affords random copolymers with molecular weight from 64 to 97 × 10³ g mol⁻¹, unimodal molecular weight distribution (2.1 < M_w/M_n < 2.6), and 1-octene content from 6.5 to 9.0 mol%. Among the two pyridine complexes, *i.e.*, **2a** and **2c**, the latter gives the copolymer with the lowest comonomer incorporation likely because the increased steric and repulsive interaction of bulky 1-octene and bulkier ligand **c** (Figure 6).

2a was then screened for the copolymerization of ethylene with 1-hexene and 4-methyl-1-pentene (Table 5, entries **18–20**). A dependence of activity on the comonomer was found: the activity (for all 4 min long experiments) increases in the order 4M1P (660 kg_{pol} mol_V⁻¹ h⁻¹) < OCT (1164) < HEX (1680) < P (2097 for entry **10**, Table 2). Accordingly, a dependence of copolymer composition on the comonomer was found: the comonomer incorporation in the copolymers increases in the order 4M1P (4.7 mol%) < OCT (9.0) < HEX (11.2) < P (13.7). Steric effect may be considered the factor responsible for the less efficient incorporation of bulkier, branched 4-methyl-1-pentene.

As concerns the microstructure of E/HEX copolymers, as an example, in Figure S12a the ^{13}C NMR spectrum of sample **18** (HEX = 11.2 mol%) is reported. The copolymer mainly contains isolated butyl branches, and alternated sequences.⁷⁶ Resonances clearly ascribed to two consecutive inserted 1-hexene units, and tiny ones due to the blocky 1-hexene repeating units are also present in the ^{13}C NMR spectrum. Finally, resonances at 25.4 and 36.2 ppm assigned to $S_{\beta\gamma}$ and $T_{\gamma\delta}$, respectively, are also visible in the spectrum: these peaks can be ascribed to 2,1-insertion of 1-hexene, leading to four uninterrupted methylene sequences ($x_{n,4}$). In Figure S12b the ^{13}C NMR spectrum of E/OCT copolymer (entry **15**, OCT = 9.0 mol%) is reported. The spectrum shows all the microstructural features found for E/HEX copolymer.

Figure 10 shows the spectrum of a selected E/4M1P copolymer (Table 5, entry **19**, 4M1P = 4.7 mol%). Copolymer resonances were assigned according to the literature: methyl, methylene and methine carbons in the side chains were designated as $\text{CH}_3(\text{sc})$, $\text{CH}_2(\text{sc})$ and $\text{CH}(\text{sc})$.⁷⁷ Beside the signal corresponding to long methylene sequences ($S_{\delta\delta}$ at 27.73 ppm), characteristic resonances at 42.5, 23.75 and 21.18 ppm corresponding to the $\text{CH}_2(\text{sc})$, $\text{CH}(\text{sc})$ and $\text{CH}_3(\text{sc})$ of the EYE triad, respectively, and characteristic resonances at 32.5, 28.2 and 24.8 ppm corresponding to $S_{\alpha\delta}$, $S_{\gamma\delta}$, and $S_{\beta\delta}$, respectively, and belonging to the same YEEE sequence, are observed. Moreover, two very small but diagnostic resonances at 21.8 ppm, and in the region around 24.5 ppm were detected and assigned to the $S_{\beta\beta}$ methylene carbons belonging to the completely alternating EYEYE and YYEYZ (Z means Y or E) pentads, respectively. Looking in more detail, the peak at about 24.5 ppm is split into two peaks at 24.5 and 24.6 ppm (see the magenta inset in the Figure 10), which can be attributed to the *meso* and *racemic* alternating sequence, respectively. Specifically, the resonance at 24.6 ppm had been assigned to the $S_{\beta\beta}$ in the *meso* alternating sequence (*m*-YEY), while the upfield resonance at 24.5 ppm to the $S_{\beta\beta}$ in the *racemic* alternating sequence (*r*-YEY). The second feature to be highlighted is the presence of some resonances due to regioirregularities.⁷⁷

Figure 10. ^{13}C NMR spectrum (in $\text{C}_2\text{D}_2\text{Cl}_4$ at 103°C , reference to HDMS) of a selected poly(ethylene-co-4-methyl-1-pentene) (Table 5, entry **19**, 4M1P = 4.7 mol%). It should be noted that the methyls at 20.6 ppm of 2MA can hardly be evaluated since their peak overlaps with other resonances likely ascribed to chain start alkane groups (marked with an asterisk). In bold a 2,1-inserted 4M1P unit. The inset magenta spectrum highlights the resonance at 24.5 ppm, assigned to $S_{\beta\beta}$ in the *meso* alternating sequence *m*-YEY, and that at 24.6 ppm belonging to $S_{\beta\beta}$ in the *racemic* alternating sequence *r*-YEY. P = growing polymer chain.



Specifically, we detected the peak at 25.3 ppm ascribed to the $S_{\beta\gamma}$ (see the green inset in the Figure 10) of even uninterrupted methylene sequence (four methylenes, $x_{n,4}$), which are generated by a 4-methyl-1-pentene inversion (YEY or YEEY, where Y is a 2,1 inserted 4M1P unit). Moreover, the presence of a small signal at 29.2 ppm, ascribed to the $S_{\alpha\beta}$, and at 33.9 ppm ascribed to the methine carbon $T_{\gamma\delta}$, are diagnostic of YEY (two methylenes, $x_{n,2}$) or YY sequences. The ^{13}C NMR spectrum is even more complicated by the presence of other small signals at 25.4, 26.0 and 37.2 ppm (M4, M2 and M3 in Figure 11, respectively) which, also due to the concomitant absence of the corresponding $T_{\delta\delta}$ at 35.8 ppm, can be assigned to the 2-methyl-alkyl structure (2MA).⁷⁸ The presence of such unit could be likely due to the chain-initiation reaction with the insertion of 4-methyl-1-pentene into a V-H active species, formed by an initial event of β -H elimination and subsequent chain-transfer. The presence of vinyl-end groups, as it will be discussed later, can be taken as proof of the existence of the V-H species.

Formation of a low- M_w copolymer facilitates investigation of chain-end groups by ^1H NMR. The ^1H NMR spectrum of sample **19** (Figure S13) reveals evidence for β -H elimination and 2,1-insertion. Indeed, the ^1H NMR spectrum in the olefin region shows a large number of overlapped peaks due to different chain saturations, originated by an initial event of β -H elimination following a last-inserted ethylene or comonomer unit. According to the literature,⁷⁹ distinctive ranges of chemical shift are detected and associated to vinylenes ($\text{PHC}=\text{CHR}$, from 5.4 to 5.2 ppm, where P = polymer chain, and R = $(\text{CH}_2)_2\text{CH}(\text{CH}_3)_2$), vinyls ($\text{CH}_2=\text{CHP}$, from 4.9 to 4.8 ppm formed after the last ethylene inserted unit followed by chain-transfer), and vinylidenes ($\text{CH}_2=\text{CPR}$, at 4.7 ppm). Specifically, vinylidenes are formed in the case of a primary insertion of 4-methyl-1-pentene followed by chain-transfer, while vinylenes are formed in the case of a secondary insertion of 4-methyl-1-pentene followed by chain-transfer. Comparison of the relative integrations for vinyls with respect to the sum of those ascribed to vinylenes and vinylidenes reveals that chain-transfer following 4-methyl-1-pentene insertion occurs three time more frequent than chain-transfer following ethylene insertion. In the case of E/HEX and E/OCT copolymers, all obtained from **2a**, the same ratio (vinylenes *plus* vinylidenes:vinyls) is 1.5:1.

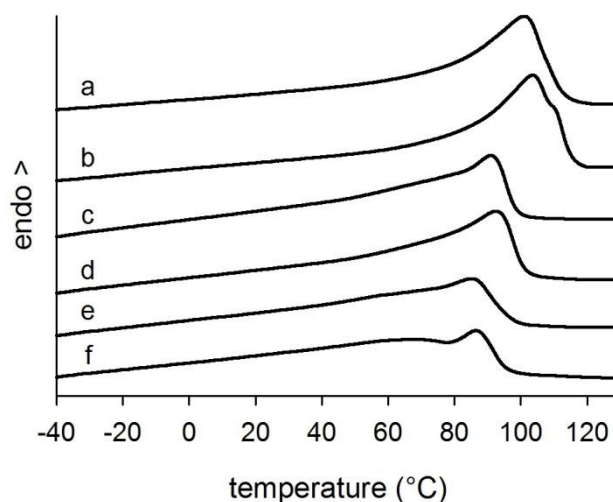
Thermal Properties

Changes in the α -olefin content and distribution affect the copolymer thermal properties. Figure 11 shows DSC heating thermograms of copolymers obtained after cooling at rate of $20\text{ }^\circ\text{C min}^{-1}$. Relevant data are summarized in Table 5.

E/4M1P copolymers containing about 5 mol% of 4M1P exhibit the highest T_m and ΔH_m values with a crystallinity around 30% (Figure 11a,b) For E/OCT copolymers, the melting event begins at lower temperatures, and may extend over a $90\text{ }^\circ\text{C}$ temperature range (Figure 11c-e). In general, as the 1-octene content increases, the melting event shifts to a lower temperature range and the melting point taken at peak maximum decreases (T_m in Table 5, entries **15–17**). Analogously, ΔH_m decreases with the comonomer content, going from 75 J g^{-1} for sample **17** (OCT = 6.5 mol%) to 58 J g^{-1} for sample **15** (OCT = 9.0 mol%), reflecting the reduced crystallinity. The E/HEX

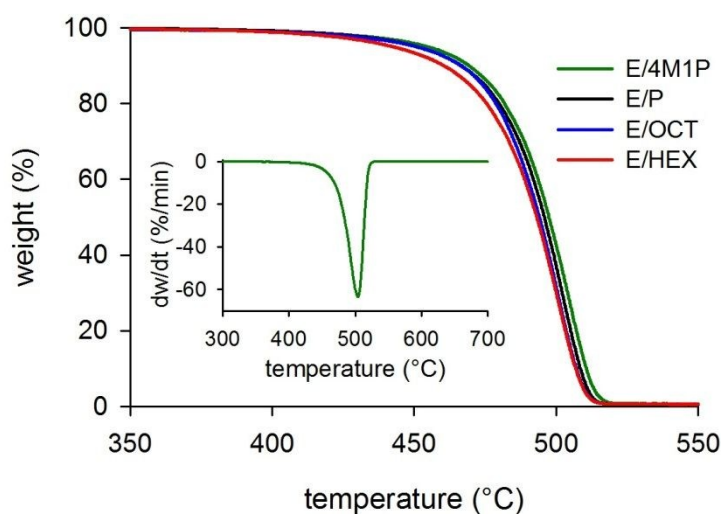
copolymer (HEX = 11.2 mol%) exhibits a broader multimodal melting endotherm with a shoulder peak before the main melting peak (Figure 11f). The broad endothermic event registered for the investigated copolymers reflects a distribution of crystalline dimensions, as a consequence of the range of different crystallizable sequence lengths in the copolymer, *i.e.* the non-uniformity in the comonomer distribution due to inter- and intramolecular compositional heterogeneity.^{80,81}

Figure 11. DSC heating scans of ethylene-*co*- α -olefin copolymers: (a) E/4M1P (entry **20**, 4M1P = 5.1 mol%), (b) E/4M1P (entry **19**, 4M1P = 4.7 mol%), (c) E/OCT (entry **16**, OCT = 6.7 mol%) (d) E/OCT (entry **17**, OCT = 6.5 mol%), (e) E/OCT (entry **15**, OCT = 9.0 mol%), (f) E/HEX (entry **18**, HEX = 11.2 mol%).



The copolymer thermal stability was investigated by TGA under inert atmosphere. In Figure 12 thermograms for samples obtained by **2a** are reported as an example. Generally, TGA curves evidence single step decomposition with a maximum rate at about 500 °C. All the copolymers were found to be thermally stable, being the initial degradation temperature corresponding to 2% mass loss ($T_{2\%}$) higher than 400 °C.

Figure 12. TGA curves of selected ethylene- α -olefin copolymers obtained by **2a**: E/4M1P (entry **19**), E/OCT (entry **15**), E/HEX (entry **18**) and E/P (entry **10**). In the inset, the TGA derivative curve of E/4M1P sample.



Mechanical Tests

Preliminary investigation on the mechanical behavior of selected copolymers obtained by **2a** was carried out at 20 °C by uniaxial stretching until failure. The stress–strain curves are shown in Figure 13A, and the tensile properties are summarized in Table 6.

The deformation of the more crystalline E/4M1P copolymer (entry **19**) proceeds with the highest Young's modulus (95 MPa), the highest tensile strength (5 MPa), and the minimum elongation before breaking (14%). Upon tensile drawing, E/HEX and E/OCT copolymers (entry **18** and **15**, respectively), having comparable molecular weight, comonomer content, and crystallinity, show significant deformation without obvious yielding, whereas the E/P copolymer (entry **10**), characterized by the highest amount of comonomer and lowest crystallinity, exhibits low Young's modulus (20 MPa) and elongation at break of about 50%. However, the mechanical behavior of these copolymers is strongly influenced by their low molecular weight. Indeed, the E/P copolymer obtained by **3d**, *i.e.*, sample **14**, with comparable propylene content, similar crystallinity, but 2.5 fold higher molecular weight with respect to sample **10**, exhibits an elastomer behavior to a certain extent with strain hardening, fracture strain higher than 800% (Figure 13B), and 33% strain recovery measured after the first step in a step cycle test at 300% strain (inset of Figure 13B).⁸²

Figure 13. (A) Stress-strain curves of selected ethylene-*co*- α -olefin copolymers obtained by **2a**: E/4M1P (entry **19**), E/OCT (entry **15**), E/HEX (entry **18**) and E/P (entry **10**), and (B) Stress-strain curve of E/P entry **14** during monotonic tensile deformation. In the inset, the stress-strain curves in the hysteresis experiment for a strain of 300%.

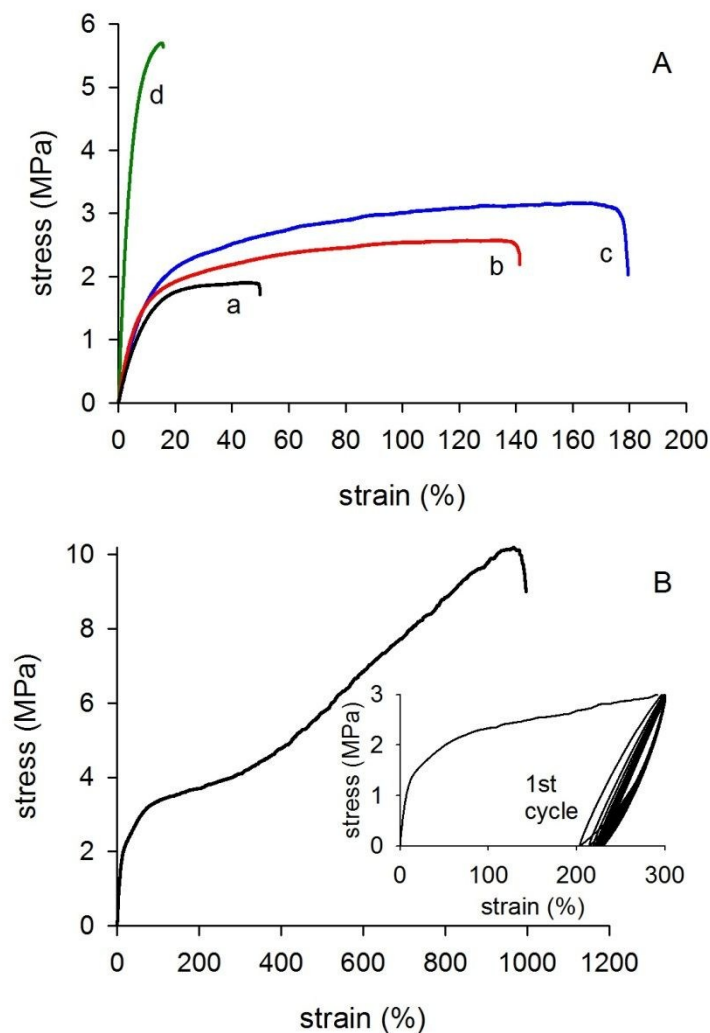


Table 6. Mechanical properties of selected E-*co*-Y copolymers

entry	Y ^a (mol%)	M _w ^b (×10 ³)	E ^c (MPa)	σ ^d (MPa)	ε ^e (%)
10	P (13.7)	98	19.6±1.1	1.8±0.1	47±10
18	HEX (11.2)	69	26.6±2.0	2.5±0.1	162±14
15	OCT (9.0)	64	25.3±0.7	3.1±0.1	181±6
19	4M1P (4.7)	55	94.7±6.8	5.2±0.5	14±2
14	P (12.4)	240	27.0±3.0	10.0±1.0	873±96

^a comonomer content determined by NMR; ^b molecular weight determined by SEC; ^c Young's modulus; ^d ultimate tensile strength; ^e elongation at break.

CONCLUSIONS

View Article Online
DOI: 10.1039/C9PY01415B

In summary, this study reports the synthesis and the characterization of a series of (imido)V(IV) complexes of general formula $V(=NR)Cl_2(NHMe_2)_2$ [$R = tBu$ (**1a**), CPh_3 (**1b**), 2,6- $CHPh_2$ -4-Cl- C_6H_2 (**1c**)], and $V(=NR)Cl_2(Py)_3$ [$R = tBu$ (**2a**), CPh_3 (**2b**), 2,6- $CHPh_2$ -4-Cl- C_6H_2 (**2c**)]. Selected **1a**, and **2a–c** were evaluated as catalyst precursors for the polymerization of ethylene, and copolymerization of ethylene with propylene, 1-hexene, 1-octene and 4-methyl-1-pentene. Polymerization tests with known PMe_2Ph -imido derivatives $V(=NR)Cl_2(PMe_2Ph)_2$ [$R = tBu$ (**3a**), iPr (**3d**)] were performed as well to evaluate the effect of the donor coligand.

In the presence of a low excess of Et_2AlCl (500 equiv to V) and ETA (10 equiv to V), **2** and **3** exhibit high initiation rate for the polymerization of ethylene, while no significant differences were observed by changing the imido ligand substitution. An exception is the dimethylamine **1a** that was much slower to initiate polymerization. However, while **1a** exhibits lower activity than pyridine and PMe_2Ph congeners, the molecular weight of the polymers from **1a** are higher than those from **2** and **3**, which may be tentatively related to concomitant accelerated chain-growth with respect to chain-transfer in the presence of a certain degree of electron donation through the dimethylamine and hence stabilization of the active site. The obtained PEs are linear polymers with T_m of about 137 °C, high molecular weight and narrow molecular weight distribution.

Introduction of the α -olefin comonomer in the reaction mixture accelerates the chain-transfer rate. Random copolymers with moderate comonomer incorporation were obtained, the comonomer reactivity being affected by the nature of the olefin and, to a lesser extent, by the imido ligand steric properties. Changes in the imido ligand substitution brought no a significant effect. The observed differences are most likely related to the kinetic: complexes having more electron-withdrawing aryl-imido substituents exhibit faster initiation rate than those with the more electron-donating tBu imido since the former, more electron-deficient, may have a pronounced preference to accept electron density from (co)monomers. All the copolymers exhibit a certain amount of inverted 2,1-inserted comonomer units so that the copolymer microstructure, particularly for poly(ethylene-*co*-

propylene)s, is described in terms of uninterrupted methylene sequences. The data obtained from NMR reveal that the electronic and steric effect of remote imido substituents shows only limited influence on the comonomer incorporation, copolymers microstructure and regioirregularities.

The thermal properties of the obtained copolymers are strongly determined by their microstructure. Comonomer content and distribution of crystallizable units along and among the polymer chains interfere on the crystallization and melting behavior. SSA thermal fractionation of poly(ethylene-*co*-propylene)s, having comparable content of propylene, reveal marked differences on the crystallizable sequence length and lamellae thickness, depending on the ligand set employed.

Conflicts of interest

There are no conflicts to declare.

Acknowledgements

We are grateful to Fulvia Greco for the acquisition of NMR spectra, Daniele Piovani for SEC measurements, and Simona Losio for fruitful discussion about the NMR spectra.

References

1. Data referred to 2017, “Plastics – The facts 2018” PlasticsEurope Market Research Group (PEMRG)/Conversio Market & Strategy GmbH.
2. M. Stürzel, S. Mihan and R. Mülhaupt, From Multisite Polymerization Catalysis to Sustainable Materials and All-Polyolefin Composites, *Chem. Rev.*, 2016, **3**, 1398–1433.
3. W. Kaminsky, Polyolefins: 50 Years After Ziegler and Natta, *Advances in Polymer Science Series*, Springer, Springer-Verlag Berlin Heidelberg, **2013**.
4. C. Chen, Designing catalysts for olefin polymerization and copolymerization: beyond electronic and steric tuning, *Nat. Rev. Chem.*, 2018, **2**, 6–14.
5. M.C. Baier, M.A. Zuideveld and S. Mecking, Post-Metallocenes in the Industrial Production of Polyolefins, *Angew. Chem. Int. Ed.*, 2014, **53**, 9722–9744.

6. J.P. McInnis, M. Delferro and T.J. Marks, Multinuclear Group 4 Catalysis: Olefin Polymerization Pathways Modified by Strong Metal–Metal Cooperative Effects, *Acc. Chem. Res.* 2014, **47**, 2545–2557. View Article Online
DOI: 10.1039/C9PY01415B
7. G.W. Coates, Precise Control of Polyolefin Stereochemistry Using Single-Site Metal Catalysts, *Chem. Rev.* 2000, **100**, 1223–1252.
8. P.S. Chum and K.W. Swogger, Olefin polymer technologies - History and recent progress at The Dow Chemical Company, *Prog. Polym. Sci.* 2008, **33**, 797–819.
9. P. Galli and G. Vecellio, Technology: Driving force behind innovation and growth of polyolefins, *Prog. Polym. Sci.* 2001, **26**, 1287–1336.
10. L. Resconi, L. Cavallo, A. Fait and F. Piemontesi, Selectivity in Propene Polymerization with Metallocene Catalysts, *Chem. Rev.* 2000, **100**, 1253–1345.
11. H. Sinn and W. Kaminsky, Ziegler-Natta Catalysis, *Adv. Organomet. Chem.* 1980, **18**, 99-149.
12. H. Sinn, W. Kaminsky, H.J. Vollmer and R. Woldt, “Living Polymers” on Polymerization with Extremely Productive Ziegler Catalysts, *Angew. Chem., Int. Ed.*, 1980, **19**, 390–392.
13. H. Makio, N. Kashiwa and T. Fujita, FI Catalysts: A New Family of High Performance Catalysts for Olefin Polymerization. *Adv. Synth. Catal.*, 2002, **344**, 477-493.
14. D. Peng, X. Yan, C. Yu, S. Zhang and X. Li, Transition metal complexes bearing tridentate ligands for precise olefin polymerization, *Polym. Chem.*, **2016**, **7**, 2601-2634.
15. B.L. Small, Discovery and Development of Pyridine-bis(imine) and Related Catalysts for Olefin Polymerization and Oligomerization, *Acc. Chem. Res.* 2015, **48**, 2599–2611.
16. J. Klosin, P.P. Fontaine and R. Figueroa, Development of Group IV Molecular Catalysts for High Temperature Ethylene- α -Olefin Copolymerization Reactions, *Acc. Chem. Res.*, 2015, **48**, 2004–2016.
17. C. Bariashir, C. Huang, G.A. Solan and W.-H. Sun, Recent advances in homogeneous chromium catalyst design for ethylene tri-, tetra-, oligo- and polymerization, *Coord. Chem. Rev.* 2019, **385**, 208–229.

18. G. Leone, E. Groppo, G. Zanchin, G.A. Martino, A. Piovano, F. Bertini, J. Martí-Rujas, E. Parisini, G. Ricci, Concerted Electron Transfer in Iminopyridine Chromium Complexes: Ligand Effects on the Polymerization of Various (Di)olefins, *Organometallics*, 2018, **37**, 4827–4840. View Article Online
DOI: 10.1039/C9PY01415B
19. F. Wang and C. Chen, A continuing legend: the Brookhart-type α -diimine nickel and palladium catalysts, *Polym. Chem.*, 2019, **10**, 2354–2369.
20. E. Junghanns, O. Gumboldt and G. Bier, Polymerization of ethylene and propylene to amorphous copolymers with catalysts of vanadium oxychloride and alkyl aluminum halides, *Makromol. Chem.*, 1962, **58**, 18–42
21. D.L. Christman and G.I. Keim, Reactivities of Nonconjugated Dienes Used in Preparation of Terpolymers in Homogeneous Systems, *Macromolecules*, 1968, **1**, 358–363.
22. K. Nomura and Zhang, Design of Vanadium Complex Catalysts for Precise Olefin Polymerization, *Chem. Rev.* 2011, **111**, 2342–2362.
23. J.Q. Wu and Y.S. Li, Well-defined vanadium complexes as the catalysts for olefin polymerization, *Coord. Chem. Rev.* 2011, **255**, 2303–2314.
24. S. Gambarotta, Vanadium-based Ziegler–Natta: challenges, promises, problems, *Coord. Chem. Rev.*, 2003, **237**, 229–243.
25. P. Groch, K. Dziubek, K. Czaja, M. Białek and D. Man, Tri-alkenyl polyhedral oligomeric silsesquioxanes as comonomers and active center modifiers in ethylene copolymerization catalyzed by bis(phenoxyimine) Ti, Zr, V and V salen-type complexes, *Appl. Catal., A*, 2018, **567**, 122–131.
26. C. Redshaw, Vanadium procatalysts bearing chelating aryloxides: Structure–activity trends in ethylene polymerization, *Dalton Trans.*, 2010, **39**, 5595–5604.
27. Y. Liu, H.-X. Xiang, K.-T. Wang, G. Wu and Y.-B. Li, Efficient Preparation of Cyclic Olefin Copolymers with Unreacted Double Bonds by Using Thermal Stable Non-Metallocene Vanadium Catalytic System, *Macromol. Chem. Phys.* **2019**, 1900008.
28. M. Białek and E. Bisz, Dichlorovanadium(IV) diamine-bis(phenolate) complexes for ethylene (co)polymerization and 1-olefin isospecific polymerization, *J. Catal.*, 2018, **362**, 65–73.

29. S.-y. Xu, X.-m Chen, L.-c Huang, F. Li and W. Gao, Vanadium chlorides supported by BIAN (BIAN = bis(arylimo)-acenaphthene) ligands: Synthesis, characterization, and catalysis on ethylene polymerization, *Polyhedron*, 2019, **16**, 146–151. View Article Online
DOI: 10.1039/C9PY01415B
30. G. Leone, I. Pierro, G. Zanchin, A. Forni, F. Bertini, A. Rapallo and G. Ricci, Vanadium(III)-catalyzed copolymerization of ethylene with norbornene: Microstructure at tetrad level and reactivity ratios, *J. Mol. Catal. A: Chem.*, 2016, **424**, 220–231.
31. G. Zanchin, I. Pierro, E. Parisini, J. Martí-Rujas, G. Ricci and G. Leone, Synthesis, structure and behavior of vanadium(III) diphosphine complexes in the homo- and co-polymerization of ethylene with norbornene: the ligand donor strength and bite angle make the difference, *J. Organomet. Chem.*, 2018, **861**, 142–150.
32. G. Zanchin, A. Gavezzoli, F. Bertini, G. Ricci and G. Leone, Homo- and Copolymerization of Ethylene with Norbornene Catalyzed by Vanadium(III) Phosphine Complexes, *Molecules*, 2019, **24**, 2088.
33. W. Ochędzan-Siodłak, A. Bihun-Kisiel, D. Siodłak, A. Poliwoda and B. Dziuk, Titanium and vanadium catalysts with oxazoline ligands for ethylene-norbornene (co)polymerization, *Eur. Polym. J.*, 2018, **106**, 148–155.
34. S. Zhang, W.C. Zhang, D.D. Shang and X.Y. Wu, Synthesis of ultra-high-molecular-weight ethylene-propylene copolymer via quasi-living copolymerization with N-heterocyclic carbene ligated vanadium complexes, *J. Polym. Sci., Part A: Polym. Chem.*, 2019, **57**, 553–561.
35. G. Zanchin, L. Vendier, I. Pierro, F. Bertini, G. Ricci, C. Lorber and G. Leone, Homo- and co-polymerization of ethylene with cyclic olefins catalyzed by phosphine adducts of (imido)vanadium(IV) complexes, *Organometallics*, 2018, **37**, 3181–3195.
36. D.C. Bradley and M.H. Gitlitz, Metallo-organic compounds containing metal–nitrogen bonds. Part VI. Infrared and nuclear magnetic resonance of dialkylamidoderivatives of titanium, vanadium, zirconium, niobium, hafnium, tantalum, and thorium, *J. Chem. Soc. A*, **1969**, 980–984.

37. C. Lorber, R. Choukroun and B. Donnadieu, Synthesis and Crystal Structure of Unprecedented Phosphine Adducts of d¹-Aryl Imido–Vanadium(IV) Complexes, *Inorg. Chem.*, 2003, **42**, 673–675. View Article Online
DOI:10.1039/C9PY01415B
38. S. Dai, X. Sui and C. Chen, Highly Robust Palladium(II) α -Diimine Catalysts for Slow-Chain-Walking Polymerization of Ethylene and Copolymerization with Methyl Acrylate, *Angew. Chem. Int. Ed.*, 2015, **54**, 9948–9953.
39. C. Lorber, R. Choukroun and B. Donnadieu, Synthesis and Structure of a Series of New d¹-Aryl Imido–Vanadium(IV) Complexes Stabilized by N-Donor Ligands, *Inorg. Chem.*, 2002, **41**, 4216–4226.
40. J. Loliger and R. Scheffold, Paramagnetic moment measurements by NMR. A micro technique, *J. Chem. Educ.*, 1972, **49**, 646–647.
41. A.G. Simanke, R.G. Alamo, G.B. Galland and R.S. Mauler, Wide-angle X-ray scattering of random metallocene-ethylene copolymers with different types and concentration of comonomer, *Macromolecules*, 2001, **34**, 6959–6971.
42. A.J. Müller, R.M. Michell, R.A. Pérez and A.T. Lorenzo, Successive Self-nucleation and Annealing (SSA): correct design of thermal protocol and applications, *Eur. Polym. J.*, 2015, **65**, 132–154.
43. Agilent Technologies (2011). Agilent Technologies UK Ltd., O., UK, Xcalibur CCD system, CrysAlisPro Software system, Version 1.171.35.19.
44. CrysAlis CCD, CrysAlis RED and associated programs: Oxford Diffraction (2006). Program name(s). Oxford Diffraction Ltd, Abingdon, England.
45. SAINT Bruker (2007). Bruker AXS Inc., Madison, Wisconsin, USA.
46. A. Altomare, G. Cascarano, C. Giacovazzo and A. Guagliardi, Completion and refinement of crystal structures with SIR92, *J. Appl. Crystallogr.*, 1993, **26**, 343–350.
47. SHELX97 [Includes SHELXS97, SHELXL97, CIFTAB] - Programs for Crystal Structure Analysis (Release 97-2). G. M. Sheldrick, Institut für Anorganische Chemie der Universität, Tammanstrasse 4, D-3400 Göttingen, Germany, (1998).

48. L.J. Farrugia, WinGX suite for small-molecule single-crystal crystallography, *J. Appl. Crystallogr.*, 1999, **32**, 837–838. [View Article Online](#)
DOI: 10.1039/C9401415B
49. *International tables for X-Ray crystallography*, Vol IV, Kynoch press, Birmingham, England, 1974.
50. L.J. Farrugia, ORTEP-3 for Windows - a version of ORTEP-III with a Graphical User Interface (GUI), *J. Appl. Crystallogr.*, 1997, **30**, 565–569.
51. C. Lorber, Titanium and vanadium imido-bridged complexes, *Coord. Chem. Rev.*, 2016, **308**, 76–96.
52. C. Lorber and L. Vendier, Novel aspects of the transamination reaction between $\text{Ti}(\text{NMe}_2)_4$ and primary amines, *Dalton Trans.*, 2013, **42**, 12203–12219.
53. C. Lorber and L. Vendier, Tight Encapsulation of a “Naked” Chloride in an Imidotitanium Hexanuclear Host, *Inorg. Chem.*, 2013, **52**, 4756–4758.
54. C. Lorber and L. Vendier, Imido-Bridged Homo- and Heterobimetallic Complexes, *Inorg. Chem.*, 2011, **50**, 9927–9929.
55. A.Y. Khalimon, E. Peterson, C. Lorber, L.G. Kuzmina, J.A.K. Howard, A. van der Est and G.I. Nikonov, Imido-Supported Borohydrides of Titanium, Vanadium and Molybdenum, *Eur. J. Inorg. Chem.*, 2013, 2205–2211.
56. A.W. Addison, T.N. Rao, J. Reedijk and J.V. van Rijn, Synthesis, structure, and spectroscopic properties of copper(II) compounds containing nitrogen–sulphur donor ligands; the crystal and molecular structure of aqua[1,7-bis(N-methylbenzimidazol-2'-yl)-2,6-dithiaheptane]copper(II) perchlorate, *J. Chem. Soc., Dalton Trans.*, 1984, 1349–1356.
57. C. Lorber, B. Donnadieu and R. Choukroun, Synthesis and X-ray characterization of a monomeric Cp-free d^1 -imido–vanadium(IV) complex, *Dalton Trans.*, 2000, 4497–4498.
58. L. Falivene, R. Credendino, A. Poater, A. Petta, L. Serra, R. Oliva, V. Scarano and L. Cavallo, SambVca 2. A Web Tool for Analyzing Catalytic Pockets with Topographic Steric Maps, *Organometallics*, 2016, **35**, 2286–2293.

59. SambVca 2.0: a web application for analyzing catalytic pockets View Article Online
DOI: 10.1039/C9PY01415B
<https://www.molnac.unisa.it/OMtools/sambvca2.0/>.
60. E. Adisson, A. Deffieux, M. Fontanille and K. Bujadoux, Polymerization of ethylene at high temperature by vanadium-based heterogeneous Ziegler–Natta catalysts. II. Study of the activation by halocarbons, *J. Polym. Sci., Part A: Polym. Chem.*, 1994, **32**, 1033–1041.
61. J.C. Randall, Methylene Sequence Distribution and Number Average Lengths in Ethylene-Propylene Copolymers, *Macromolecules*, 1978, **11**, 33–36.
62. C. Redshaw, M.A. Rowan, D.M. Homden, S.H. Dale, M.R.J. Elsegood, S. Matsui and S. Matsuura, Vanadyl C and N-capped tris(phenolate) complexes: influence of pro-catalyst geometry on catalytic activity, *Chem. Comm.* 2006, 3329–3331.
63. C. Redshaw, M.J. Walton, M.R.J. Elsegood, T.J. Prior and K. Michiue, Vanadium(V) tetraphenolate complexes: synthesis, structural studies and ethylene homo-(co-)polymerization capability, *RSC Adv.*, 2015, **5**, 89783–89796.
64. C. Redshaw, M. Walton, K. Michiue, Y. Chao, A. Walton, P. Elo, V. Sumerin, C. Jiang and M.R.J. Elsegood, Vanadyl calix[6]arene complexes: synthesis, structural studies and ethylene homo-(co-)polymerization capability, *Dalton Trans.*, 2015, **44**, 12292–12303.
65. S. Zhang, W.-C. Zhang, D.-D. Shang, Z.-Q. Zhang and Y.-X. Wu, *Dalton Trans.*, 2015, **44**, 15264–15270.
66. X. Hao, C. Zhang, L. Li, H. Zhang, Y. Hu, D. Hao and X. Zhang, Use of Vanadium Complexes Bearing Naphthalene-Bridged Nitrogen-Sulfonate Ligands as Catalysts for Copolymerization of Ethylene and Propylene, *Polymers*, 2017, **9**, 325.
67. C. Cuomo, S. Milione and A. Grassi, Olefin polymerization catalyzed by amide vanadium(IV) complexes: The stereo- and regiochemistry of propylene insertion, *J. Polym. Sci., Part A: Polym. Chem.*, 2006, **44**, 3279–3289.

68. C.J. Carman and C.E. Wilkes, Monomer Sequence Distribution in Ethylene/Propylene Elastomers. I. Measurement by Carbon-13 Nuclear Magnetic Resonance Spectroscopy, *Rubber Chem. Technol.* 1971, **44**, 781–804. View Article Online
DOI: 10.1039/C9PY01415B
69. W.-J. Wang and S. Zhu, Structural Analysis of Ethylene/Propylene Copolymers Synthesized with a Constrained Geometry Catalyst, *Macromolecules*, 2000, **33**, 1157–1162.
70. V.B.F. Mathot, Ch. C. M., Fabrie, Chain structure of homogeneous ethylene-propylene copolymers showing inversion, described on the basis of ^{13}C -NMR data. I. Theory. *J. Polym. Sci., Part B: Polym. Phys.* **1990**, *28*, 2487.
71. S. Mansel, U. Rief, M.-H. Prosenc, R. Kirsten and H.-H. Brintzinger, *ansa*-Metallocene derivatives XXXII. Zirconocene complexes with a spiro-silane bridge: syntheses, crystal structures and properties as olefin polymerization catalysts, *J. Organomet. Chem.*, **1996**, *512*, 225–236.
72. L. Mandelkern, Crystallization of polymer, Equilibrium Concepts vol. 1, Cambridge University Press, 2002.
73. M. Keating, I.H. Lee, C.S. Wong, Thermal fractionation of ethylene polymers in packaging applications, *Thermochim. Acta* 284 (1996) 47–56.
74. Kong, X. Fan, Y. Xie, W. Qiao, Study on molecular chain heterogeneity of linear low density polyethylene by cross-fractionation of temperature rising elution fractionation and successive self-nucleation/annealing thermal fractionation, *J. Appl. Polym. Sci.* 94 (2004) 1710–1718.
75. F. Zhang, Q. Fu, T. Lu, H. Huang, T. He, Improved thermal fractionation technique for chain structure analysis of ethylene/ α -olefin copolymers, *Polymer* **2002**, *43*, 1031–1034.
76. J. C. Randall, C-13 nuclear magnetic-resonance quantitative measurements of monomer sequence distribution in hydrogenated polybutadienes, *J. Polym. Sci., Part B: Polym. Phys.*, 1975, **13**, 1975–1990.
77. S. Losio, A.C. Boccia and M.C. Sacchi, Ethylene/4-Methyl-1-pentene Copolymers by a “Constrained Geometry Catalyst”: Advances in ^{13}C NMR Assignment, *Macromol. Chem. Phys.*, 2008, **209**, 1115–1128.

78. S. Losio, G. Leone, F. Bertini, G. Ricci, M.C. Sacchi and A.C. Boccia, Ethylene–4-methyl-1-pentene copolymers of complex chain architecture using a-diimine Ni(II) catalysts: synthesis, ¹³C NMR assignment and understanding the chain-walking mechanism, *Polym. Chem.* 2014, **5**, 2065–2075.
79. V. Busico, R. Cipullo, N. Friederichs, H. Linssen, A. Segre, V. Van Axel Castelli and G. van der Velden, H NMR Analysis of Chain Unsaturation in Ethene/1-Octene Copolymers Prepared with Metallocene Catalysts at High Temperature, *Macromolecules*, 2005, **38**, 6988–6996.
80. M. Canetti, G. Leone, G. Ricci, F. Bertini, Structure and thermal properties of ethylene/4-methyl-1-pentene copolymers: Effect of comonomer and monomer sequence distribution, *Eur. Polym. J.* 2015, **73**, 423–432.
81. G. Leone, M. Canetti, I. Pierro, G. Zanchin, C. De Rosa, G. Ricci, F. Bertini, (Micro)structure, thermal behavior and mechanical properties of ethylene–propylene–1-octadecene terpolymers from chain-walking polymerization of 1-octadecene, *Polymer* 2019, **166**, 27–37.
82. Y. Guo, Z. Fu, J. Zu, Z. Fan, Structure and properties of ethylene/propylene copolymers synthesized with bis(2,4,7-trimethylindenyl)zirconium dichloride activated by methyl aluminoxanes containing different amount of trimethylaluminum, *Polymer* 2017, **122**, 77–86.

